Spatial and temporal multiyear sea ice distributions in the Arctic: A neural network analysis of SSM/I data, 1988–2001

Gennady I. Belchansky
Space Monitoring and Ecoinformation Systems Sector, Institute of Ecology, Russian Academy of Sciences, Moscow, Russia

David C. Douglas
U.S. Geological Survey, Juneau, Alaska, USA

Ilia V. Alpatsky and Nikita G. Platonov
Space Monitoring and Ecoinformation Systems Sector, Institute of Ecology, Russian Academy of Sciences, Moscow, Russia

Received 16 March 2004; revised 1 June 2004; accepted 3 August 2004; published 30 October 2004.

[1] Arctic multiyear sea ice concentration maps for January 1988–2001 were generated from SSM/I brightness temperatures (19H, 19V, and 37V) using modified multiple layer perceptron neural networks. Learning data for the neural networks were extracted from ice maps derived from Okean and ERS satellite imagery to capitalize on the stability of active radar multiyear ice signatures. Evaluations of three learning algorithms and several topologies indicated that networks constructed with error back propagation learning and 3-20-1 topology produced the most consistent and physically plausible results. Operational neural networks were developed specifically with January learning data, and then used to estimate daily multiyear ice concentrations from daily-averaged SSM/I brightness temperatures during January. Monthly mean maps were produced for analysis by averaging the respective daily estimates. The 14-year series of January multiyear ice distributions revealed dense and persistent cover in the central Arctic surrounded by expansive regions of highly fluctuating interannual cover. Estimates of total multiyear ice area by the neural network were intermediate to those of other passive microwave algorithms, but annual fluctuations and trends were similar among all algorithms. When compared to Radarsat estimates of multiyear ice concentration in the Beaufort and Chukchi Seas (1997–1999), average discrepancies were small (0.9–2.5%) and spatial coherency was reasonable, indicating the neural network's Okean and ERS learning data facilitated passive microwave inversion that emulated backscatter signatures. During 1988–2001, total January multiyear ice area declined at a significant linear rate of -54.3×10^3 km^2 yr^{-1} (-1.4% yr^{-1}). The most persistent and extensive decline in multiyear ice concentration (-3.3% yr^{-1}) occurred in the southern Beaufort and Chukchi Seas. In autumn 1996, a large multiyear ice recruitment of over 10^6 km^2 (mostly in the Siberian Arctic) fully replenished the previous 8-year decline in total area, but it was followed by an accelerated and compensatory decline during the subsequent 4 years. Seventy-five percent of the interannual variation in January multiyear sea ice area was explained by linear regression on two atmospheric parameters: the previous winter's (JFM) Arctic Oscillation index as a proxy to melt duration and the previous year's average sea level pressure gradient across the Fram Strait as a proxy to annual ice export. Consecutive year changes (1994–2001) in January multiyear ice volume were significantly correlated with duration of the intervening melt season ($R^2 = 0.73$, -80.0 km^3 d^{-1}), emphasizing a large thermodynamic influence on the Arctic's mass sea ice balance during summers with anomalous melt durations. *INDEX TERMS:* 1640 Global Change: Remote sensing; 4207 Oceanography: General: Arctic and Antarctic oceanography; 4215 Oceanography: General: Climate and interannual variability (3309); *KEYWORDS:* SSM/I, ERS, Okean, passive microwave, multiyear, sea ice

Citation: Belchansky, G. I., D. C. Douglas, I. V. Alpatsky, and N. G. Platonov (2004), Spatial and temporal multiyear sea ice distributions in the Arctic: A neural network analysis of SSM/I data, 1988–2001, *J. Geophys. Res.*, *109*, C10017, doi:10.1029/2004JC002388.

0148-0227/04/2004JC002388$09.00

1. Introduction

[2] Arctic geophysical processes play an important role in maintaining the thermodynamic balance of Earth's climate system. Arctic sea ice is a fundamental component of the system, and understanding climate variability and trends requires accurate information about sea ice dynamics and its numerous feedback processes [*Manabe et al.*, 1992; *Barry*, 1990; *Barry et al.*, 1993; *Thompson and Wallace*, 1998; *Holland*, 2001; *Parkinson et al.*, 2001; *Kukla*, 2004]. Sea ice modulates climate by influencing the short wave albedo, heat, moisture, and momentum between the atmosphere and ocean [*Agnew*, 1993; *Chapman and Walsh*, 1993; *Deser and Blackmon*, 1993; *Deser et al.*, 2002]. Sea ice is also characterized by unexpected and significant interannual variability [*Walsh and Johnson*, 1979; *Hibler and Becky*, 1985; *Fang and Wallace*, 1994; *Mysak et al.*, 1996; *Deser et al.*, 2000].

[3] Changes and trends in Arctic sea ice cover have been rigorously investigated during the recent decade using passive microwave data [*Chapman and Walsh*, 1993; *Maslanik et al.*, 1996; *Parkinson et al.*, 1999; *Gloersen et al.*, 1999; *Vinnikov et al.*, 1999; *Kwok and Rothrock*, 1999; *Johannessen et al.*, 1999; *Parkinson and Cavalieri*, 2002; *Comiso*, 2001, 2002a, 2002b]. However, validation studies have indicated varying amounts of seasonal and regional biases in SMMR and SSM/I sea ice concentration estimates [*Maslanik*, 1992; *Emery et al.*, 1994; *Kwok et al.*, 1996; *Comiso and Kwok*, 1996; *Comiso et al.*, 1997], especially with respect to multiyear (MY) sea ice concentration estimates derived with the NASA Team algorithm [*Belchansky and Douglas*, 2002]. Because MY ice dominates the thickness distribution of Arctic sea ice and influences ice-albedo feedbacks [*Curry et al.*, 1995], accurate data about long-term trends and interannual dynamics of the MY ice fraction are needed to improve climate models [*Rind et al.*, 1995, 1997; *Holland and Curry*, 1999; *Steele et al.*, 2001; *Hewitt et al.*, 2001; *Holland and Bitz*, 2003, *Kukla*, 2004].

[4] Specific problems for accurately estimating sea ice parameters are common to all active/passive microwave sensors because the reflection/emission of sea ice depends nonlinearly on numerous factors such as dielectric properties, density, homogeneity, surface roughness, sensor frequency and polarization, and sensor look-angle [*Cavalieri et al.*, 1990a; *Fung*, 1994]. However, because sensitivities among different microwave sensors vary across different surface types and surface conditions, employing multisensor algorithms allows the strengths of one sensor to compensate for some deficiencies of another [*Belchansky and Douglas*, 2000]. Among different methods, artificial neural networks (NN) are robust candidates to improve existing sea ice classification techniques because they are able to approximate a wide class of functions without a priori assumptions about their distribution laws, and build decision surfaces of any configuration using a learning process [*Hecht-Nielsen*, 1987].

[5] In this paper, we present a comparative evaluation of MY sea ice inversions of SSM/I brightness temperature (Tb) data using different multiple layer perceptron (MLP) neural networks that were constructed with learning data extracted from ERS synthetic aperture radar (SAR) and Okean MY ice map products. We evaluate different neural network learning algorithms and topologies for their ability to produce consistent and plausible estimates of multiyear ice concentration, we evaluate performance of the Okean and ERS derived learning data, and we assess the impact of learning data errors.

[6] Next, we present and discuss the observed results, a 14-year series of January mean multiyear sea ice concentration maps. Although the methodology was applicable to any winter period, we selected the mid-winter month of January to evaluate and debut the neural network results because microwave sea ice signatures are most stable during frozen conditions [*Comiso and Kwok*, 1996; *Belchansky and Douglas*, 2002]. Comparisons are made with other passive microwave and active radar estimates of MY ice cover. We then examine interannual changes in MY ice cover at regional scales, followed by an investigation of the mechanisms that affect temporal fluctuations, and conclude with an assessment of thickness and volume changes. In our discussions, we often speculate about processes and mechanisms with the intent to illustrate how information about MY ice dynamics might improve scientific understanding of the integrated ocean-ice-atmosphere system. To this end, we are currently constructing a longer time series of observational MY ice data sets by adapting the neural network methodology to all winter months of the entire SSMR-SSM/I record (1979 to present).

2. Methods

2.1. Study Area

[7] Neural networks for estimating multiyear sea ice concentration were developed, assessed, and applied within the full extent (60.21°N, 120.96°W; 63.58°N, 29.05°E; 55.22°N, 169.51°W; 57.96°N, 83.16°E) of the geographic area shown in Figure 1. A two-pixel buffer zone was applied to a Northern Hemisphere land mask (25-km resolution, obtained from NASA Goddard Space Flight Center) to eliminate land-to-ocean Tb spillover. In section 3.5, analyses were restricted to the Arctic Ocean, which included adjacent parts of the Laptev, East Siberian, Chukchi, and Beaufort Seas (Figure 1). The Arctic Ocean region encompassed approximately 6.04×10^6 km^2 of the total pelagic area (9.33×10^6 km^2) delimited in Figure 1.

2.2. Satellite Data

[8] Defense Meteorological Satellite Program SSM/I Daily Gridded Brightness Temperatures [*Maslanik and Stroeve*, 1992] and Daily and Monthly Polar Gridded Sea Ice Concentrations [*Comiso*, 1990a; *Cavalieri et al.*, 1990b] were acquired for 9 July 1987 to 31 December 2001 from the National Snow and Ice Data Center (NSIDC), Boulder, Colorado. We used daily total ice concentrations and MY ice concentrations derived with the Bootstrap and NASA Team algorithms, respectively [*Comiso et al.*, 1997]. The NSIDC data were distributed in polar stereographic projection (central meridian 45°W, latitude of true scale 70°N) with 25 km × 25 km pixel size. We standardized the SSM/I Tb data sets by correcting for instrument drift, reducing the influences of atmospheric weather conditions and coastal boundaries, and eliminating or interpolating missing data as described by *Cavalieri et al.* [1999]. We also applied linear regression coefficients to standardize intersatellite Tb cali-

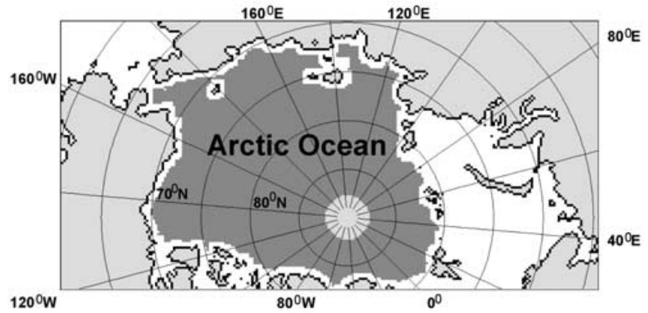

Figure 1. Geographic extent of the entire study area and the region defined as Arctic Ocean (dark shading).

brations: F13 SSM/I to F11 SSM/I [*Stroeve et al.*, 1998], and F8 SSM/I to F11 SSM/I [*Abdalati et al.*, 1995].

[9] Okean passive microwave (36.62 GHz H, 500-km swath, 15-km resolution) and side-looking radar (9.52 GHz VV, 450-km swath, 1.5-km resolution) images were acquired from the Scientific Research Center for Natural Resources (Dolgoprudny, Moscow District) during January 1996 (27 images), January 1997 (22 images), May 1997 (17 images), and January 1998 (4 images). The Okean raw passive microwave and radar images were radiometrically calibrated, equalized, and projected to polar stereographic coordinates. Concentrations of MY ice, first-year (FY) ice, and open water (OW) were estimated within a 3 km × 3 km pixel-resolution grid using linear mixture modeling of the measured backscattering cross section (σ^0) and Tb values [*Belchansky and Douglas*, 2000]. Simultaneous analysis of passive microwave and backscatter data improved separation of the ice classes. The ice-type coefficients for the mixture model were visually estimated at the centroids of three data clusters (MY, FY, and OW) evident on a two-dimensional plot of the σ^0 and Tb pixels values, thus providing independent image-specific tie-points for each scene. The Okean ice maps were averaged daily within a 25 km × 25 km resolution grid identical to the SSM/I data sets, and the MY ice concentration estimates were extracted for the neural network learning data set.

[10] Multiyear sea ice concentration estimates derived from ERS SAR data by the Geophysical Processor System [*Kwok and Cunningham*, 1993] were obtained from the Alaska SAR Facility, Fairbanks, Alaska. The ERS σ^0 images had been individually processed and were disseminated as 100 km × 100 km ice maps with 5-km pixel size in polar stereographic projection. For network learning, the ERS MY ice concentration maps for January 1992 (n = 1725) and January 1993 (n = 107) were averaged daily within a 25-km resolution grid identical to the SSM/I data sets.

2.3. Neural Network Inversion of SSM/I Data

[11] An artificial neural network defines a computational architecture for complex data processing using sets of many simple processors called neurons. In a multilayer network, all neurons are decomposed into non-overlapping subsets (layers) that are interconnected through activation functions parameterized by neuron weights and bias coefficients. Network topology defines the structure of neuron connections, and network learning is the iterative task of parameterizing the activation functions to obtain the best approximation with minimal error.

[12] However, practical use of neural networks for multichannel satellite data analysis is complicated by interactions between the choice of learning algorithm and the necessity to account for spectral, spatial, textural, and statistical properties of the images during classification. Accuracy of each learning algorithm is influenced by its ability to find the global minima of the error function while maintaining its ability to generalize the selected learning data. For any applied task lacking a priori documentation, conducting a thorough (albeit time consuming) evaluation of learning algorithm efficacy is paramount to obtaining sound results. Consequently, we present details of our learning algorithm assessment in this paper to facilitate prospective neural network studies of multiyear sea ice using passive microwave data.

[13] Three feed-forward artificial MLP neural networks were developed and evaluated to estimate MY sea-ice concentrations, each using three SSM/I Tb channels (19H, 19V, and 37V) for input data and Okean and ERS MY ice concentration maps for learning data. The three SSM/I Tb input channels were selected to standardize comparisons with other traditionally used passive microwave algorithms that discriminate MY ice. The three neural networks were each developed with a different learning algorithm: (1) error back propagation and simulated annealing [*Kirkpatrick*, 1983]; (2) dynamic learning with polynomial basis functions [*Tzeng et al.*, 1994] and Kalman filtering [*Kalman and Bucy*, 1961]; and (3) dynamic learning with two-step optimization and Kalman filtering. These three learning algorithms are subsequently referred to as: M1, M2, and M3, respectively. Topology of each neural network was defined with one input layer (n = 3 nodes: SSM/I Tb 19H, 19V, and 37V), p hidden layers (n_i artificial neurons in every ith hidden layer, $i = 1, 2, 3, \ldots, p$), and one output layer (n = 1 node: MY ice concentration) (Figure 2).

[14] In practice, we implemented a modified neural network structure that provided higher degree approximations using relatively fewer hidden neurons compared to the simply connected MLP network illustrated in Figure 2 [*Fung*, 1994]. In each modified neural network, the activation functions of the output layer were linear, and output neurons were connected with all input and hidden neurons. Output of the modified neural network can be characterized as a linear weighted sum. The error function for N learning data sets can be written as

$$E = \sum_{j=1}^{N} \left(d^j - \mathbf{W}\mathbf{x}^j\right)^T \left(d^j - \mathbf{W}\mathbf{x}^j\right), \qquad (1)$$

where $\mathbf{W}\mathbf{x}^j$ is the output signal of the neural network obtained after processing the $\mathbf{x}$ vector from the learning data set j, and d^j corresponds to the desired value of the output signal for the $\mathbf{x}$ vector from the learning data set j.

[15] The M1 learning algorithm was based on error back propagation and simulated annealing [*Kirkpatrick*, 1983] with random assignment of the step-direction through tunable parameters. The algorithm executed the first learning iteration with random initialization of the tunable parameters. The possibility to perform gradient descending

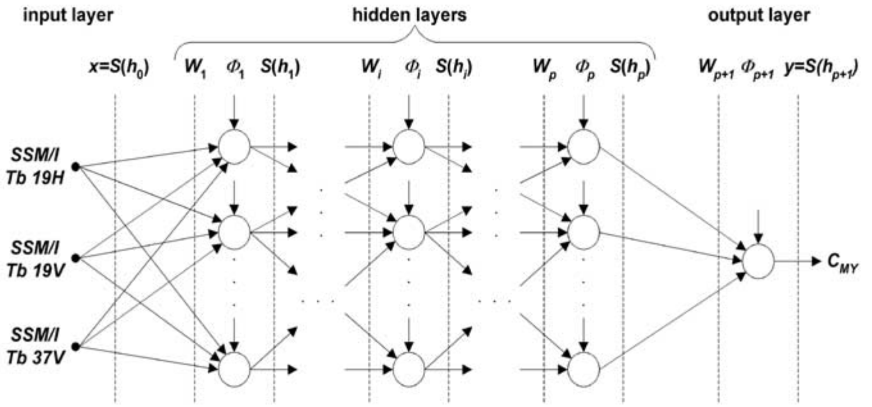

Figure 2. Topology of the multiple layer perceptron feed-forward artificial neural network.

was estimated at every step based on analysis of the error functional. In the case of a successful step (the error functional value decreased) the iteration would finish; otherwise, simulated annealing was performed. After each iteration completed, a stopping criterion was checked, and if it was not fulfilled, the next iteration was executed.

[16] The M2 learning algorithm was based on a compressed MLP model where the output was represented as a weighted sum of polynomial compositions [*Tzeng et al.*, 1994]. Since the output signal was a linear function of weights, to minimize the error functional during learning, only linear equations required solution. Adaptive Kalman filtering was implemented to calculate the network weighting vectors using recurrent equations [*Kalman and Bucy*, 1961]. Initial values of the network weights were assumed to be a set of small positive numbers.

[17] The M3 learning algorithm decomposed the learning process into linear and nonlinear optimization steps. The linear step used the dynamic learning algorithm M2. After the adaptive Kalman filtering had estimated the matrix of weighting coefficients (**W**), the estimates were refined using a simple second-order minimization scheme based on the Newton-Raphson method [*Barton*, 1991]. Keeping all other parameters fixed, small positive and negative changes were made in one parameter, and the step required to move to the quadratic minimum was calculated by expanding equation (1) as a truncated Taylor series. The presence of maxima and oscillations were tested for and avoided.

2.4. Evaluation of Learning Algorithms

[18] Experiments were conducted to evaluate the relative performance of each neural network learning algorithm (M1, M2, and M3). Two internally different neural network topologies were also evaluated for each learning algorithm: 3-20-1 and 3-16-4-1. These two topologies were selected for evaluation following extensive predevelopment trials. Topologies with minimal internal layers were considered first, and then the number of neurons in the internal levels and the number of levels was increased, and so on. The procedure was executed until a reasonable accuracy of inversion was attained, and a reasonable learning time on the previous step was achieved. Commonly, during the task of inversion, a complex topology caused the network to lose its ability to generalize the learning results, while too few hidden neurons led the network to limited sensitivity of the learning process.

[19] Two Okean multiyear ice concentration (C_{MY}) maps dated 4 May 1997 were selected as learning data sets for the evaluation. A springtime period was chosen to maximize representation of sea ice types and surface melt conditions. Although ultimate application of the neural network was intended for winter months, we challenged the learning algorithms with a "worst case" scenario to expose their robustness to novel or anomalous environmental conditions. Geographic extent of the Okean learning data encompassed good representation of the study area's total 4 May 1997 SSM/I Tb variability (Figure 3). The combined 4 May 1997 Okean C_{MY} data were randomly divided with equal probability into two data sets: learning and testing, each with approximately 2000 samples (pixels). The randomization procedure was independently repeated 10 times to create 10 pairs of learning and testing data sets. Each learning and testing data set pair was used with each combination of learning algorithm (M1, M2, M3) and topology (3-20-1, 3-4-16-1) to create a total of 60 neural networks.

[20] When compared to the Okean C_{MY} source maps, the neural network C_{MY} estimates generated during learning versus testing were similar in magnitude and dispersion among all learning algorithms and topologies (Table 1). The similarity indicated that representation of the MY ice environment in the learning data set was sufficient for all algorithms and topologies to perform equally well within the geographic extent of learning data. However, further evaluations were warranted to assess each algorithm's performance in regions beyond the geographic bounds of the learning data, because it is inappropriate to assess the quality of a neural network based solely on errors associated with restricted learning data sets. Therefore, each of the 60 neural networks was used to estimate C_{MY} throughout the full study area on 4 May 1997.

[21] Despite apparently good representation of the learning data (Figure 3), the learning algorithms and topologies performed differently in areas outside the learning data boundaries (Figure 4). Among the 10 replications, the error back propagation and simulated annealing learning algorithm (M1) with 3-20-1 topology produced the most consistent C_{MY} estimates throughout the study area, while the dynamic learning algorithms (M2 and M3) and the 3-16-4-1

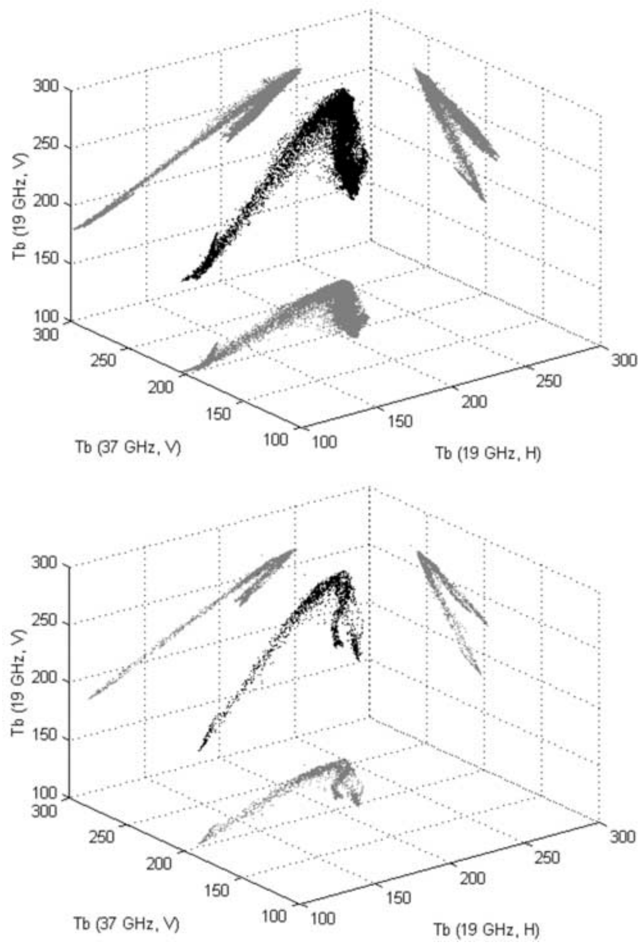

Figure 3. Projected three-dimensional scatterplots of SSM/I Tbs over Arctic sea ice on 4 May 1997; (top) SSM/I pixels for the entire study area and (bottom) SSM/I pixels corresponding to the area encompassed by two Okean learning data sets used for assessing the neural network learning algorithms and topologies.

topology manifested distinct regions with pronounced C_{MY} variability. Although all algorithms and topologies produced fairly similar and acceptable results within the region of learning data (Table 1, Figure 4), the M1 learning algorithm with 3-20-1 topology produced the most physically plausible and correspondent C_{MY} estimates across the entire study area.

[22] Hemispheric-scale sea ice inversion from passive microwave data presents challenges and difficulties because relationships are highly nonlinear [*Fung*, 1994], and fully representative learning data are lacking. Kalman filtering is useful for approximating the third-power polynomial, but only if the learning data are ideally representative (sufficient volume spanning the whole approximation area) and accurate (without noise); otherwise the network risks losing its ability to generalize. Because the M2 and M3 learning algorithms employed Kalman filtering, and both resulted in discordant and sometimes physically implausible C_{MY} estimates, the third-power polynomial approximations were probably overfitting the "less-than-ideal" learning data.

[23] We concluded that error back propagation with simulated annealing (M1) was a more robust learning algorithm by its ability to construct a "smooth" neural network for estimating C_{MY} throughout the entire Arctic, especially given the impracticality of assembling an ideal representation of learning samples over such a large and heterogeneous geographic area. Consequently, we used the M1 learning algorithm and 3-20-1 topology for all subsequent analyses and evaluations.

2.5. Evaluation of Learning Data

[24] All January Okean C_{MY} learning data (n = 13563 pixels, 25-km pixel resolution, Figure 5) were pooled and then randomly divided into a learning and testing data set pair. The randomization procedure was repeated 10 times to create 10 data set pairs. The M1 learning algorithm with 3-20-1 topology was applied to each of the learning data set pairs to construct a total of 10 neural networks. The learning data evaluations were conducted by examining C_{MY} estimates for a single day. Each network was used to estimate C_{MY} throughout the study area on 15 January 1988–2001, by inverting the respective three-channel SSM/I Tb daily image data (10 replicates estimating C_{MY} on 15 January in each of 14 years). Analogous methods were applied to the full set of January ERS learning data (n = 2572 pixels, 25-km pixel resolution, Figure 5).

[25] Relative merits of Okean versus ERS learning data were evaluated by comparing the C_{MY} means and variances among the 10 testing replicates in each year. All 14 years demonstrated similar results, so 1993 was arbitrarily selected for illustration. The neural networks derived from ERS learning data produced consistent C_{MY} estimates in high-latitude regions, but grossly overestimated C_{MY} in southern regions (Figure 6). Because the combined January ERS learning data set was dominated by sea ice in the northern Beaufort Sea (Figure 5), the derivative neural networks were inherently specific to high C_{MY} conditions, but poorly provisioned to estimate low C_{MY} throughout the marginal zones. Although the geophysical properties of sea ice are known to vary over broad regions of the Arctic [*Tucker et al.*, 1992], failure of the ERS neural network was most likely caused by insufficient representation of low C_{MY} in the learning data.

[26] In contrast, the January Okean learning data were more proportionally balanced over a broader latitudinal gradient of ice types, concentrations, and environmental conditions (Figure 5), rendering more robust networks and producing more reasonable and consistent C_{MY} estimates throughout the full study area. However, within the high-latitude regions of contiguous multiyear ice, C_{MY} estimates

Table 1. Mean (and Standard Deviation) Root Mean Square (RMS) Differences Between Two 4 May 1997 Okean Multiyear Sea Ice Concentration Maps and Their Derivative Neural Network (NN) Estimates Obtained by 10 Learning and Testing Replications, for Each of Three Learning Algorithms (M1, M2, M3) and Two Topologies

	NN Topology 3-20-1				NN Topology 3-16-4-1			
	RMS_{LEARN}		RMS_{TEST}		RMS_{LEARN}		RMS_{TEST}	
M1	8.14%	(0.45)	8.57%	(0.48)	7.91%	(0.54)	8.41%	(0.44)
M2	8.68%	(0.42)	8.89%	(0.51)	8.49%	(0.49)	8.81%	(0.38)
M3	8.36%	(0.41)	8.64%	(0.45)	8.42%	(0.45)	8.75%	(0.44)

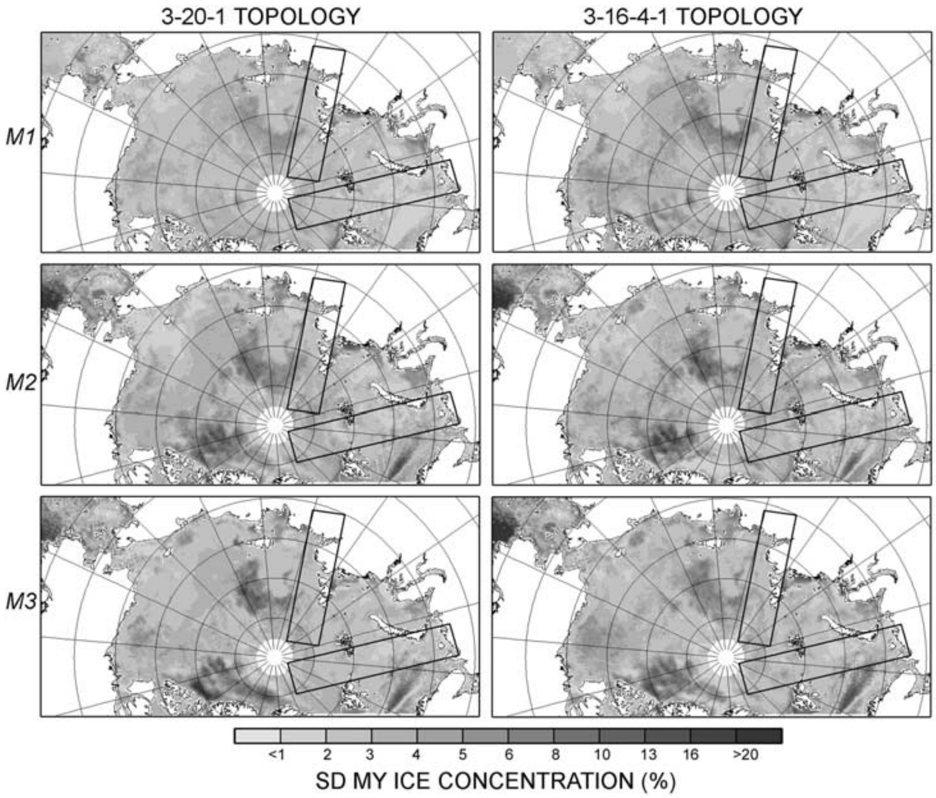

Figure 4. Standard deviation (SD) of MY sea ice concentration estimates ($N = 10$ replications) obtained by neural networks constructed with two different topologies and three different learning algorithms. Rectangles delineate boundaries of the 4 May 1997 Okean MY ice concentration learning data sets.

by the ERS neural networks had consistently less variability than those obtained with the networks based on Okean learning data (Figure 6).

[27] Assuming that (1) the Okean learning data may have slightly overestimated C_{MY} in high C_{MY} ranges [*Belchansky and Douglas*, 2002], (2) the C_{MY} estimates based on ERS learning data had better consistency and hence better accuracy in high C_{MY} ranges (Figure 6), and (3) the C_{MY} estimates based on ERS learning data overestimated C_{MY} in low C_{MY} ranges (Figure 6), we concluded it reasonable to construct a merged C_{MY} map that capitalized on respective strengths of the Okean and ERS learning data sets. Accordingly, the 10 Okean and 10 ERS daily C_{MY} maps were, respectively, averaged, and a single merged C_{MY} daily map (Okean-ERS) was conditionally constructed,

$$\begin{aligned} &\mathrm{C_{OKEAN\text{-}ERS}} = \mathrm{C_{OKEAN}} \quad && \mathrm{C_{OKEAN}} < \mathrm{C_{ERS}}, \\ &\mathrm{C_{OKEAN\text{-}ERS}} = \mathrm{C_{ERS}} && \mathrm{C_{OKEAN}} \geq \mathrm{C_{ERS}}, \end{aligned} \tag{2}$$

$$\begin{aligned} &\mathrm{SD_{OKEAN\text{-}ERS}} = \mathrm{SD_{OKEAN}} \quad && \mathrm{C_{OKEAN}} < \mathrm{C_{ERS}}, \\ &\mathrm{SD_{OKEAN\text{-}ERS}} = \mathrm{SD_{ERS}} && \mathrm{C_{OKEAN}} \geq \mathrm{C_{ERS}}. \end{aligned} \tag{3}$$

If the above assumptions were correct, then errors associated with the C_{MY} estimates in the merged map would be lower than the errors of either source map.

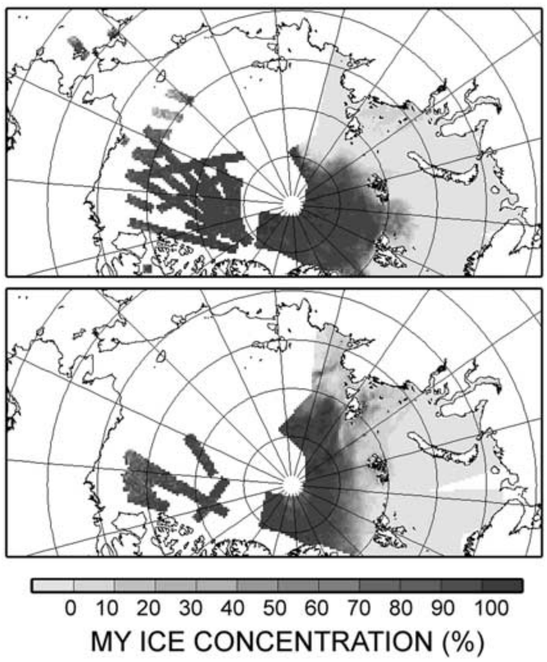

Figure 5. Composite distributions of (top) January 1996 and (bottom) 1997 ERS and Okean multiyear sea ice concentration learning data: ERS Geoprocessing System maps (Beaufort and Chukchi Seas) and Okean linear mixture model maps (Barents, Kara, and Laptev Seas).

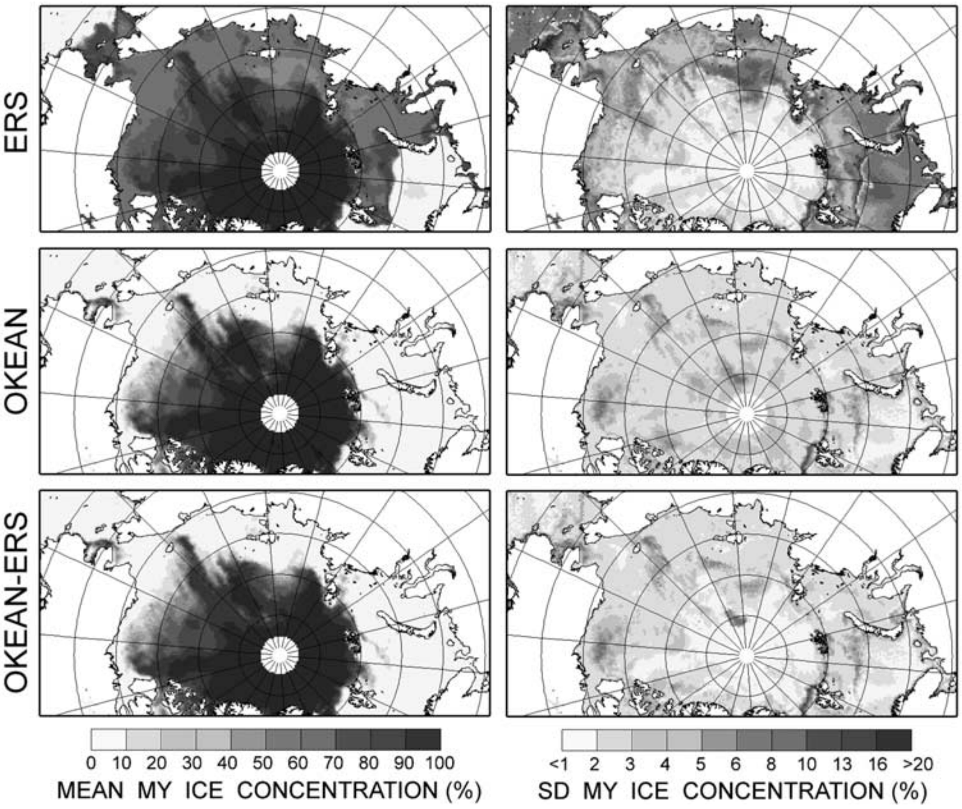

Figure 6. Mean and standard deviation multiyear (MY) sea ice concentration estimates, 15 January 1993, by 10 neural network replications based on (top) ERS learning data, (middle) Okean learning data, and (bottom) conditional merging of the ERS and Okean estimates.

2.6. Construction of Monthly Mean Maps

[28] For each day in January, the 10 Okean and 10 ERS neural networks described above were used to produce 20 daily C_{MY} maps by inverting the respective daily SSM/I Tb three-channel inputs (19V, 19H, and 37V). The resulting 10 Okean and 10 ERS C_{MY} daily map-replicates were respectively averaged, then merged ($C_{OKEAN\text{-}ERS}$) using equation (2), and then averaged within years to produce January mean C_{MY} maps, 1988–2001. All results presented henceforth were based on analyses of the January mean C_{MY} estimates.

2.7. Evaluation of Neural Network Estimates

[29] Accuracy of the Okean and ERS C_{MY} learning data is clearly important to accuracy of the derivative neural network C_{MY} estimates. Accuracy assessments of sea ice parameters estimated by remote sensing methods are largely deficient because definitive validation data are lacking, especially for studies that discriminate ice age. Comparative assessments are more common, where coincident estimates derived from one sensor or algorithm are contrasted with another. Direct comparisons between the Okean and ERS C_{MY} learning data were not possible since the data did not overlap. However, *Belchansky and Douglas* [2002] found that total ice concentration estimates derived by the Okean linear mixture model averaged 1.4% (sd = 5.9) higher in January compared to Radarsat ScanSAR estimates derived by σ^0 image segmentation. Also, ERS C_{MY} estimates derived with look-up tables and maximum likelihood classification averaged 3.8% (sd = 7.4) less than those obtained using supervised classification, while an iterative maximum likelihood algorithm used operationally by the GPS reduced the discrepancy to 1.0% (sd = 6.1) [*Fetterer et al.*, 1994].

[30] We investigated sensitivity of the neural network C_{MY} estimates to errors in Okean and ERS learning data by comparing the original C_{MY} estimates to those obtained with new neural networks constructed from learning data that contained simulated errors. Using results from *Fetterer et al.* [1994] to establish liberal estimates of variance and bias, we offset each Okean and ERS C_{MY} learning data pixel by a random amount ranging uniformly between −10% and +18% (mean +4%). A uniform distribution was chosen to exacerbate the introduced error. Offsets resulting in <0% or >100% were truncated. New Okean and ERS neural networks were developed with the simulated learning data, and then applied to construct new monthly mean C_{MY} maps for January 1996.

[31] Minor differences were observed between the original Okean-ERS C_{MY} estimates and those derived from the learning data with simulated errors (Table 2). Variance of the differences was commensurate to that of the simulated noise, indicating that the network's learning algorithm and topology were robust against amplification of errors in the learning data. Restricting the simulated error to just the Okean or ERS learning data showed that the Okean-ERS C_{MY} estimates were more sensitive to

Table 2. Mean (and Standard Deviation) Differences Between Average January (1996) Multiyear Ice Concentration Estimates Derived From Neural Networks That Were Constructed Using the Original Okean and ERS Learning Data Versus Networks Constructed With Learning Data That Contained Simulated Errors (Okean* and ERS*)[a]

	Full Study Area	Arctic Ocean
Okean-ERS minus Okean*-ERS*	−0.6% (5.8)	−1.4% (4.3)
Okean-ERS minus Okean*-ERS	−0.7% (5.9)	−1.6% (4.5)
Okean-ERS minus Okean-ERS*	−0.3% (1.8)	0.6% (1.0)

[a]N = 14,542 pixels (Full Study Area); N = 9292 pixels (Arctic Ocean).

errors in the Okean learning data (Table 2). A greater sensitivity to errors in the Okean learning data was expected since Okean-derived network estimates tended to dominate the ERS-derived estimates when the two products were merged (equation (2)). Mean differences were a few percent less than the simulated +4% bias, suggesting that the Okean-ERS neural network may have slightly underestimated multiyear ice concentrations relative to the learning data.

3. Results and Discussion

3.1. Interannual Distributions

[32] January mean MY ice distributions were relatively stable in the western central Arctic and highly variable throughout the peripheral regions during 1988–2001 (Figure 7). Variance among the 14-year series of January MY ice distribution maps (Figure 7, bottom right) delineated a discrete region of dense and persistent MY ice cover located north of the Canadian Arctic Archipelago and the north Greenland coast that is maintained by the consolidating forces of the Beaufort gyre and the Transpolar Drift Stream [*Erlingsson*, 1988; *Rigor et al.*, 2002]. An expansive peripheral zone of highly variable C_{MY} conditions surrounded the consolidated region. Within the peripheral zone, consecutive year fluctuations of multiyear ice cover at regional scales were often maximal (presence-absence).

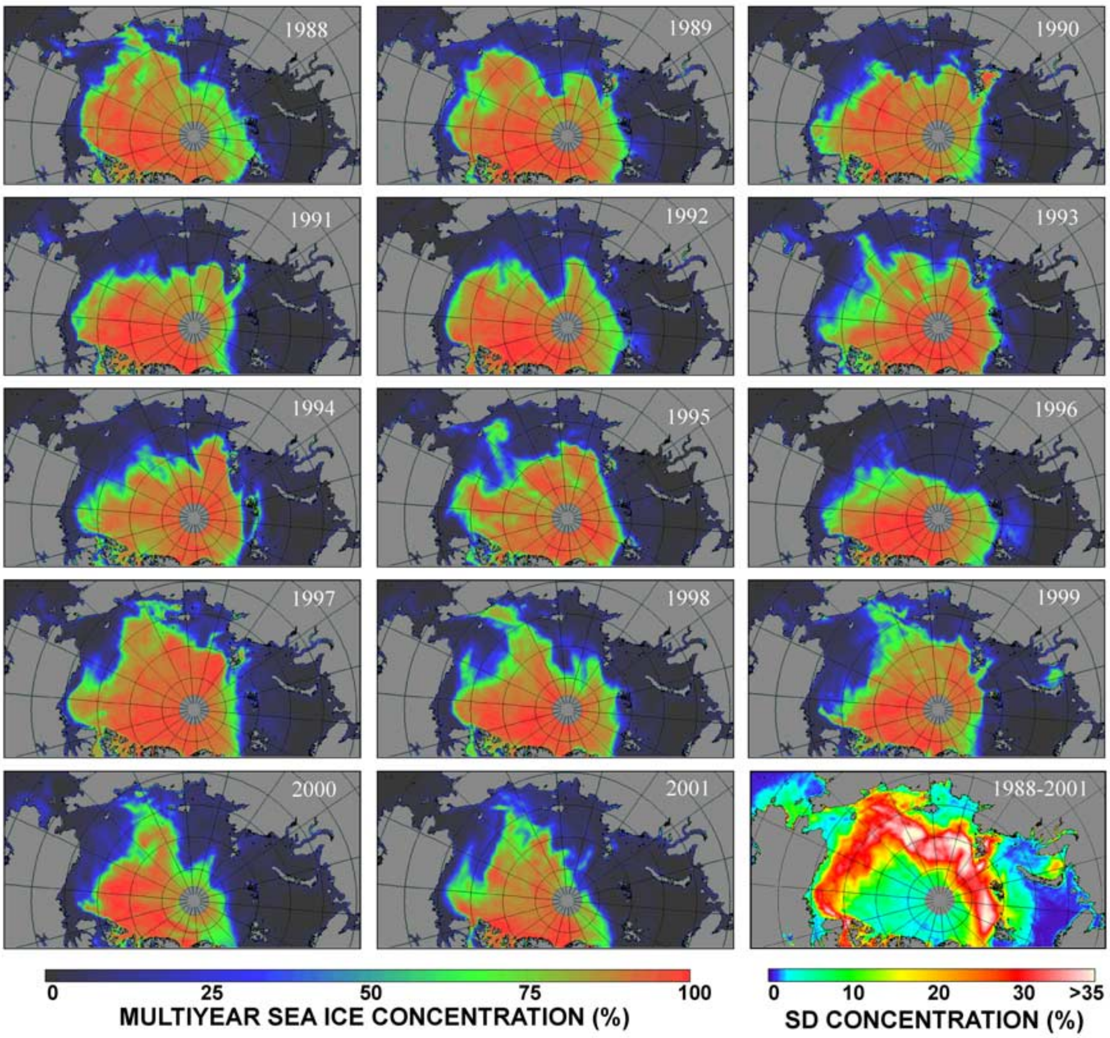

Figure 7. January mean multiyear sea ice concentration estimates, 1988–2001, based on neural network inversions of daily SSM/I passive microwave brightness temperatures (19V, 19H, 37V). The 14-year standard deviation is shown in the bottom right panel.

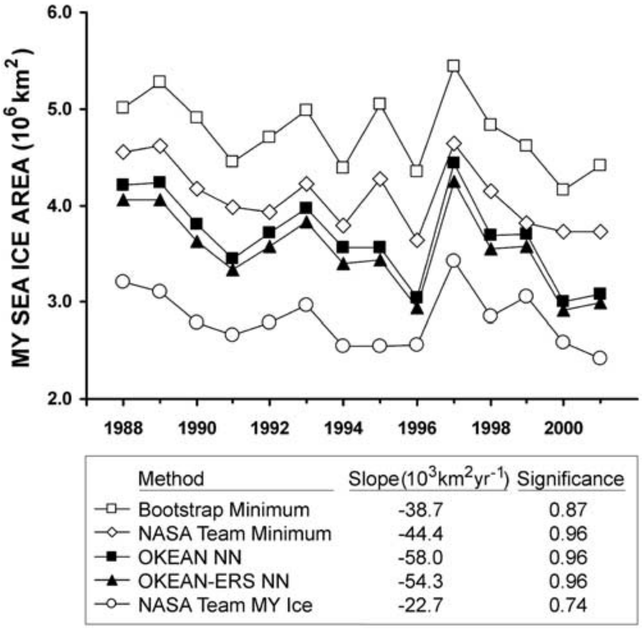

Figure 8. Annual mean multiyear (MY) sea ice area estimates and linear trends (1988–2001) obtained by five different methods of SSM/I passive microwave analysis: previous-year total ice area minimas by the Bootstrap and NASA Team algorithms, and current year January multiyear ice area estimates by the Okean-ERS neural network, Okean neural network, and the NASA Team MY algorithm.

[33] The pronounced C_{MY} variability throughout the peripheral zone manifests a complex integration of seasonal MY ice recruitment, melt, and transport. During winter, surface air temperature, wind, water temperature, snow cover, thermohaline stratification, and mechanical rafting and ridging dictate the development and physical character of first-year ice [*Thomas and Dieckmann*, 2003]. Winter conditioning of first-year ice is important to its probability of surviving variable summer melt conditions and becoming recruited as MY ice the following winter. Concurrently, wind-driven forces associated with variable synoptic [*Maslanik et al.*, 1996] and oscillatory atmospheric circulations [*Rigor et al.*, 2002] dominate patterns of sea ice motion, transporting ice into regions with different thermal regimes or exporting it entirely from the Arctic basin. Large interannual variations in regional C_{MY} distributions also imply correspondent variations to sea ice thickness distributions [*Winsor*, 2001; *Holloway and Sou*, 2002].

3.2. Comparative Trends

[34] Previous passive microwave studies of MY ice have used two distinct strategies to estimate area, extent, and trends. One strategy uses linear combinations of the 18- or 19-GHz and 37-GHz Tb channels, and requires "tie points" to guide discriminations between water, first-year ice, and multiyear ice signatures. The most common examples are the NASA Team algorithm [*Gloersen and Cavalieri*, 1986] and the NORSEX algorithm [*Svendsen et al.*, 1983]. Principal drawbacks of these classification algorithms stem from unaccounted spatial and temporal variations in the MY ice signature caused by the geophysical influences of dynamic surface temperatures [*Grenfell*, 1992] that are not well represented by a static set of tie points. The second strategy is parsimoniously premised on the assumption that each year the total sea ice at the end of the summer melt season (annual minima) depicts MY ice by definition [*Comiso*, 1990b]. This approach possesses a distinct advantage because it precludes problems associated with ice type classification, but it is limited to a single observation of MY distribution each year. In comparison, the neural network approach embodies several notable advantages: (1) it exploits the stability of MY ice signatures derived from active radar instruments [*Kwok et al.*, 1996]; (2) it accommodates nonlinear relationships between the input and output variables [*Fung*, 1994; *Kwok et al.*, 1996]; (3) it is inherently calibrated to the seasonal conditions of broad geographic areas, as represented in the learning data; and (4) it can be used to investigate intraseasonal dynamics by elaborating its application to other winter months.

[35] We compared our neural network estimates of multiyear ice area to those derived with other passive microwave algorithms: the NASA Team MY ice algorithm and both the Bootstrap and NASA Team algorithms for estimating total ice during the summer minima. For each method, we calculated total MY ice area by summing the product of each pixel's ice concentration estimate and area (adjusted for map distortion), for all pixels with $\geq$15% ice concentration within the full geographic extent of Figure 1. The date of minimum ice cover was annually determined using a 7-day running mean of daily total ice concentration estimates, analogous to the method ascribed by *Comiso* [2002a].

[36] The most apparent differences among the passive microwave methods were the magnitudes of the MY ice area estimates (Figure 8). On average, the Bootstrap estimates of total ice area during the previous summer minima were 26% (sd = 4.2%) higher than the neural network estimates of January MY ice area. Attaining higher MY ice area estimates during the late summer melt/freeze transition can be partly attributed to incorrectly assimilating regions of new ice, since minimum ice cover does not occur in all areas of the Arctic on the same date [*Comiso*, 2002b]. Lower MY ice area estimates in January can be partly explained by ice export during the intervening period, and to a lesser extent, ridging of relatively thin second-year ice. Other factors may have attenuated or masked the microwave signature of MY ice, such as dense atmospheric water vapor [*Maslanik*, 1992], abundant frozen melt ponds [*Grenfell*, 1992], heavy snow loads [*Cavalieri et al.*, 1991], and seawater intrusion at the snow-ice interface or over-rafting by first-year ice [*Comiso*, 1990b; *Kwok et al.*, 1996]. Also, detection of new MY ice (second-year ice) may have been problematic if it possessed transitional emissivity characteristics [*Tooma et al.*, 1975; *Grody*, 1988] that were not adequately represented in the neural network learning data. Of the average 26% difference between the estimates of total MY ice area by the Bootstrap summer minima and the Okean-ERS neural network the following January, we very roughly attribute no more than 9% to ice export [*Vinje et al.*, 1998; *Kwok and Rothrock*, 1999; G. Belchansky, unpublished data, 2004] and 6% to incorrect autumn assimilation of new ice [*Comiso*, 2002b],

Table 3. Mean (and Standard Deviation) Differences Between RGPS Estimates of January Multiyear Ice Concentration in the Beaufort-Chukchi Seas and Estimates by the Okean-ERS Neural Network and the NASA Team MY Algorithm[a]

	1997	1998	1999
RGPS minus Okean-ERS NN	2.4% (9.8)	2.5% (11.5)	0.9% (13.7)
RGPS minus NASA Team MY	18.8% (13.1)	16.7% (14.2)	11.2% (14.2)

[a] N = 4126 pixels in each year.

leaving at least 10% accountable to ice convergence, Tb signature attenuation, and/or methodological bias.

[37] The NASA Team MY ice algorithm consistently produced the lowest area estimates (Figure 8), averaging 41% (sd = 3.9%) lower than the Bootstrap estimates of total ice during the summer minima and 20% (sd = 4.4%) lower than the January neural network estimates. Previous studies have reported similar discrepancies between NASA Team MY ice concentration estimates and those derived by other algorithms and sensors [*Kwok et al.*, 1996; *Belchansky and Douglas*, 2000]. The NASA Team algorithm estimated 14% (sd = 2.4%) less total ice area during the summer minima compared to the Bootstrap algorithm, a commonly observed relationship attributed to differences between the algorithms [*Comiso et al.*, 1997].

[38] In general, the Bootstrap and NASA Team algorithms rendered similar spatial distributions of ice extent during the summer minima, but the Team algorithm consistently underestimated ice concentrations throughout all regions. Consequently, the NASA Team total area estimates for the summer minima were closer in magnitude to the January neural network MY estimates, but the similarity did not represent improved spatial congruency between their mapped C_{MY} distributions. Results of the strictly Okean-derived neural network are presented in Figure 8 to illustrate the subtle and consistent decrease (4%, sd = 0.5%) in MY ice area that resulted when the Okean and ERS C_{MY} estimates were merged with equation (2).

[39] All passive microwave methods depicted similar annual fluctuations and long-term trends among their total MY ice area estimates (Figure 8). During 1988–1996, MY ice cover diminished approximately 1.0×10^6 km^2. The decline was dramatically interrupted by complete replenishment in autumn 1996, followed by a rapid and compensatory 4-year decline. On the basis of the Okean-ERS neural network, the overall 1988–2001 linear decline in January MY ice area was -54.3×10^3 km^2 yr^{-1} (-1.4% yr^{-1}), somewhat accelerated compared to rates of other studies that included earlier years. *Comiso* [2002b] reported that Arctic MY ice area had declined -0.9% yr^{-1} during 1979–2000 based on estimates of minimum total ice cover derived with the Bootstrap algorithm, and *Johannessen et al.* [1999] reported a -31×10^3 km^2 yr^{-1} (-0.7% yr^{-1}) decline during 1979–1998 based on winter C_{MY} estimates derived with the NORSEX algorithm.

3.3. Radarsat Comparison

[40] The Radarsat geophysical processor system (RGPS) was developed to exploit the high temporal frequency of Radarsat SAR imagery for estimating motion, deformation, and thickness of the Arctic Ocean sea ice cover [*Kwok and Cunningham*, 2002]. The RGPS also produces a backscatter-based classification [*Kwok et al.*, 1992] of ice age (MY versus FY). We averaged the January RGPS C_{MY} ice products (http://www-radar.jpl.nasa.gov/rgps) for 1997, 1998, and 1999 (N = 10, 7, 10, respectively) for comparison with the corresponding January C_{MY} maps derived with the Okean-ERS neural network. Before averaging, each RGPS C_{MY} map (12.5-km pixel size) was resampled to 25-km pixel resolution (by averaging the four nearest RGPS C_{MY} values) and smoothed with a 3×3 weighted low-pass filter (1/4:1/8:1/16). Comparisons with respective Okean-ERS neural network maps were restricted (masked) to pixels where the RGPS January average had ≥ 6 samples in each of the 3 years (N = 4126 pixels).

[41] On average, the Okean-ERS neural network C_{MY} estimates were slightly less (0.9–2.5%) than those obtained by the RGPS, while the NASA Team MY algorithm reiterated its propensity to significantly underestimate MY ice concentration (Table 3). Reasonable spatial coherence was also attained between the neural network and RGPS C_{MY} maps (Figure 9). The RGPS method tended to estimate slightly higher C_{MY} than the neural network in the northern regions of contiguous MY ice. Discrepancies were most prevalent along the southernmost MY ice margin, possibly due to insufficient representation of the region in the learning data sets (Figure 5). However, the notable level of overall correspondence between the Okean-ERS neural network and RGPS C_{MY} estimates provided independent corroboration of neural network retrievals from passive microwave data. Since the Okean and ERS neural networks were constructed with learning data derived from active radar instruments, it was not surprising that the methodology emulated RGPS backscatter-based C_{MY} estimates. Incidentally, visual inspection of a mid-January 1997 map of NSCAT (scatterometer) backscatter at 40° incidence angle [*Ezraty and Cavanié*, 1999, Plate 3] indicated that areas with $\sigma^0 > 0.1$ were closely aligned to areas with >50% C_{MY} in the January 1997 neural network map (Figure 7). Apparently, using neural networks with learning data derived from active radar instruments provides a strategy to bridge continuity between C_{MY} estimates based on historical passive microwave data and those based on recent or future active radar campaigns.

3.4. Spatial Variability

[42] Interannual fluctuations and trends in MY ice cover were examined regionally by partitioning the study area (Figure 1) into six longitudinal sectors corresponding with major peripheral seas and landmasses: (1) Greenland and Canadian Archipelago (0°–120°W) and (2) Beaufort and Chukchi Seas (120°W–180°W), East Siberian Sea (180°–140°E), Laptev Sea (140°E–100°E), Kara Sea (100°E–60°E), and Barents Sea (60°E–0°).

[43] North of Greenland and Canada, the total area of MY sea ice was relatively stable during 1988–2001 (Figure 10a). Although subtle, this was the only longitudinal sector to exhibit evidence of consistent periodicity (~5-year cycle). Linear decline of MY ice area was most apparent in the Beaufort and Chukchi Seas, diminishing at a significant rate of -33.6×10^3 km^2 yr^{-1} during 1988–2001 (Figure 10b). During the 1990s, predominantly positive winter AO conditions weakened the Beaufort Gyre, causing less MY ice to

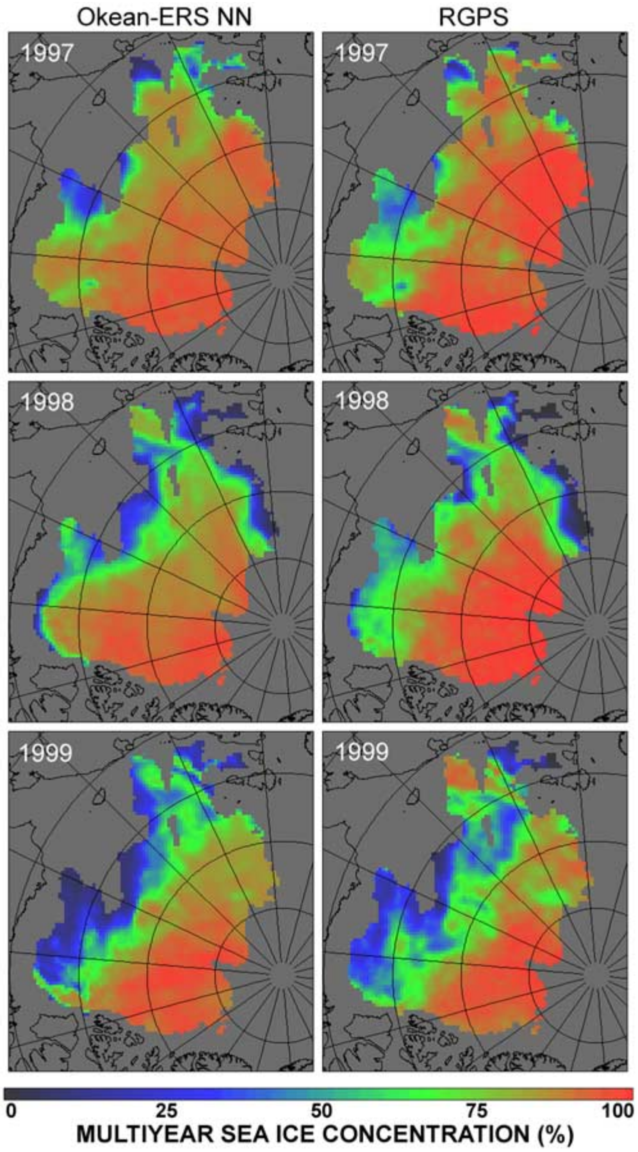

Figure 9. January mean multiyear sea ice concentration estimates (1997–1999), based on (left) daily SSM/I Tb inversion by the Okean-ERS neural network and (right) 3–6 day Radarsat σ^0 thresholding by the RGPS. Comparisons were masked to pixels where the RGPS January mean was based on $\geq$6 samples in each of the 3 years.

be transported from the western Canadian Arctic into the southern Beaufort Sea [*Drobot and Maslanik*, 2003]. The reduced southward MY ice transport is believed partly responsible for the extreme minimum ice extents recently observed in the western Arctic [*Maslanik and Serreze*, 1999; *Serreze et al.*, 2003].

[44] The East Siberian sector exhibited a marked decline in MY ice area during the early 1990s (Figure 10c) that coincided with a greater frequency of low-pressure systems during summer [*Maslanik et al.*, 1996] and longer melt seasons [*Belchansky et al.*, 2004]. The East Siberian sector gained the largest net recruitment of MY ice in autumn 1996, followed by a modest decline during the subsequent 4 years. In the Laptev Sea sector, MY ice cover was relatively constant until the mid-1990s when a shift to strong annual fluctuations developed (Figure 10d). Cause of the shift to pronounced variability is unclear, but perhaps changes in synoptic storm patterns regionally influenced the strength and trajectory of the Transpolar Drift Stream as it traversed the central Siberian Arctic (Figure 7).

[45] Multiyear ice area declined over 50% in the Kara and Barents Sea regions, culminating in 2000–2001 (Figures 10e–10f). During the 1990s, volume and temperature of Atlantic water entering the Eurasian Basin increased [*Grotefendt et al.*, 1998; *Zhang et al.*, 1998], while the insulating cold halocline layer (CHL) showed signs of significant degradation [*Steele and Boyd*, 1998]. Both mechanisms would tend to diminish winter ice production [*Dickson et al.*, 2000; *Martinson and Steele*, 2001] and reduce recruitment and maintenance of the region's MY ice. Despite recent (late 1990s) indications that the temperature of Atlantic water entering the Arctic Ocean has cooled [*Gunn and Muench*, 2001] and a weakened CHL has reestablished [*Boyd et al.*, 2002], MY ice cover in the Barents-Kara Seas reached a minimum in 2000–2001. The absence of a concurrent MY ice recovery is intriguing, and may indicate that the response of MY ice to thermohaline dynamics in the Eurasian Basin integrates cumulative conditioning over several years; however, distribution changes due to ice motion must be simultaneously considered.

[46] Alternatively, we used cluster analysis to objectively partition the observed C_{MY} variability into classes (regions) with similar interannual fluctuations in MY ice concentrations. Compared to the somewhat arbitrary longitudinal boundaries, the regions delineated by clustering expressed the data's inherent variability. A 14-band composite image was constructed in which bands were sequential years and pixel values were Okean-ERS C_{MY} estimates. An ISODATA clustering algorithm [*Ball and Hall*, 1967] was used to define six classes, commensurate with the number of

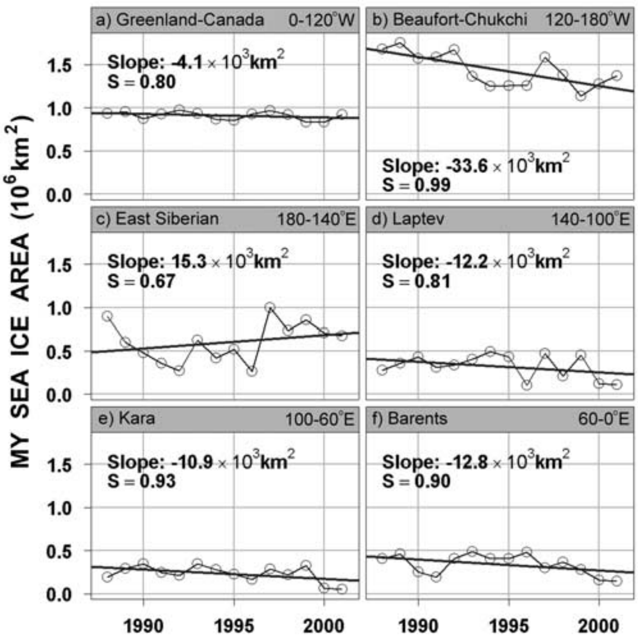

Figure 10. January mean multiyear sea ice areas and linear trends (1988–2001), within six longitudinal sectors of the study area.

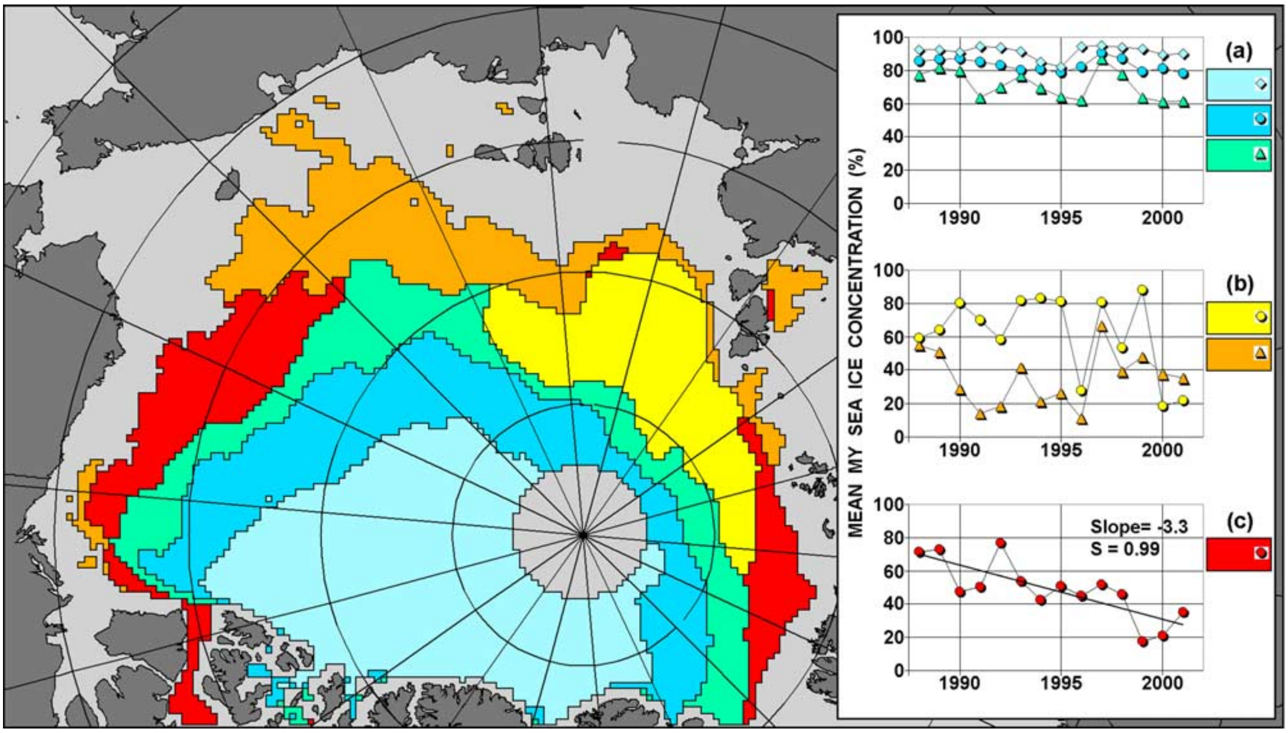

Figure 11. Six regions (classified by cluster analysis) with similar mean vectors in the 14-year chronology (1988–2001) of January multiyear (MY) ice concentration estimates derived with the Okean-ERS neural network algorithm. Class means (right) are color-coded to the mapped regions.

longitudinal sectors examined above. Pixels entering the classification were required to have at least one annual C_{MY} estimate $\geq$80% to ensure that the algorithm was not dominated by a small subset of highly variable pixels in the extreme peripheral MY ice margin.

[47] The cluster analysis revealed latitudinal gradients (Figure 11) that were dampened by the longitudinal sectors (Figure 10). Two concentric regions of MY ice bordered the periphery of the dense and stable central Arctic region: an inner region with slightly less C_{MY} and comparably low fluctuations, and an outer region with variably less C_{MY} (Figure 11a). Coherency of East Siberian and Laptev Seas regions was somewhat preserved in the cluster analysis (Figure 11b), so the ice cover fluctuations were similar to those of their respective longitudinal sectors (Figures 10c–10d). The cluster analysis emphasized pronounced and persistent C_{MY} declines (-3.3% yr^{-1}) in the southern MY ice margins of the Beaufort-Chukchi Seas and the western Eurasian Basin (Figure 11c). In the Beaufort-Chukchi Seas, the decline's southward emphasis substantiated diminished MY ice transport by a weakened Beaufort Gyre [*Drobot and Maslanik*, 2003], while reduced MY ice in the Eurasian Basin complied with both a westward and accelerated shift in the Transpolar Drift Stream [*Rigor et al.*, 2002] and/or increased ocean heat fluxes [*Grotefendt et al.*, 1998; *Steele and Boyd*, 1998].

3.5. Temporal Variability

[48] Total area of MY ice in the Arctic Ocean is annually controlled by two principal mechanisms: (1) thermodynamic recruitment or loss, governed by heat fluxes that influence winter ice growth and summer melt [*Holland et al.*, 1997; *Lindsay*, 1998; *Perovich et al.*, 2003]; and (2) dynamic loss, governed primarily by wind-driven forces that export ice through the Fram Strait [*Vinje et al.*, 1998; *Kwok and Rothrock*, 1999]. We used linear regression analyses to examine relationships between the January estimates of MY ice area within the Arctic Ocean (Figure 1) and estimates of melt season duration, export, and associated atmospheric pressure indices. We constrained analyses to the Arctic Ocean to better correspond with the area drained by the Fram Strait. The atmospheric indices likely incorporated other factors that influence MY ice area such as ridging [*Holland and Curry*, 1999] and trajectory of the Transpolar Drift Stream [*Rigor et al.*, 2002].

[49] Length of the melt season influences the probability of FY ice surviving the summer and becoming recruited as MY ice in following winter. We found a significant linear relationship between the length of the melt season (days) in FY ice [*Belchansky et al.*, 2004] and the total area of MY ice the following January ($R^2 = 0.63$, Figure 12a), but only after three outlying years (1996, 2000, 2001) were excluded (all years, $R^2 = 0.21$). *Belchansky et al.* [2004] reported that length of the melt season (melt duration) in FY ice was significantly correlated ($r = 0.74$) with the preceding winter (JFM) AO index; hence we obtained similar results when January MY ice area was regressed on the previous winter's AO index (Figure 12b).

[50] Most sea ice exported from the Arctic Ocean flows through the Fram Strait. We examined Fram Strait area fluxes reported by *Vinje et al.* [1998] for 1991–1995, and by *Kwok and Rothrock* [1999] for 1979–1995. When January MY ice area was regressed on their cumulative monthly ice area flux estimates for the previous calendar year, linear relationships were evident, but sample sizes were small (Figure 12c). *Kwok and Rothrock* [1999] found

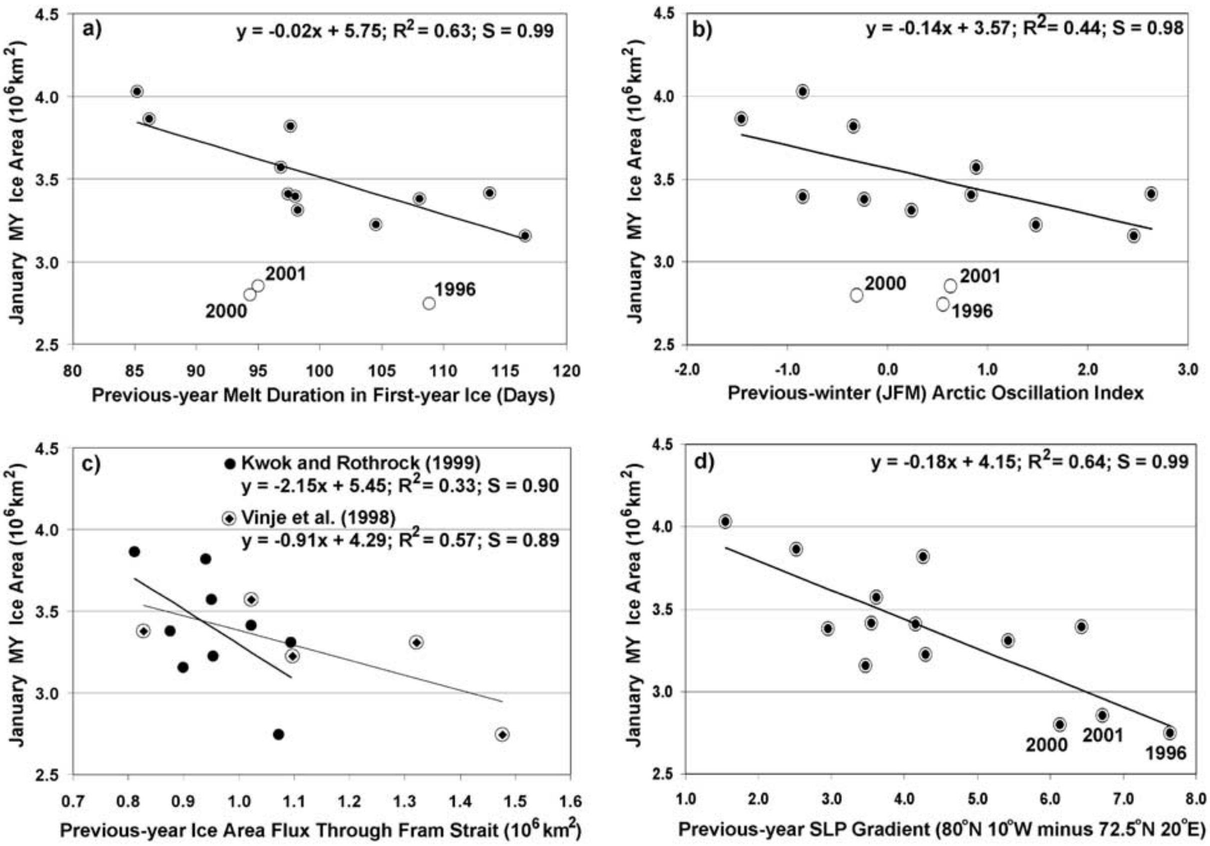

Figure 12. January multiyear ice area in the Arctic Ocean study area (Figure 1) regressed on (a) previous-year mean melt duration in FY ice, (b) previous-winter AO index, (c) previous-year cumulative ice area flux through the Fram Strait, and (d) previous-year average sea level pressure gradient across the Fram Strait. Year labels denote January MY ice area. Open symbols denote years excluded from regressions. Winter AO (JFM) indices were acquired from http://www.cpc.ncep.noaa.gov.

that ice area flux was strongly correlated (r = 0.85) with gradient sea level pressure (SLP) across the Fram Strait. We regressed January MY ice area on the previous year's average pressure difference between 80.0°N 10.0°W and 72.5°N 20.0°E [*Vinje*, 2001a] using monthly SLP data from the NCAR/NCEP 40-year Reanalysis, and found a significant linear relationship (Figure 12d) that corroborated a similar analysis presented by *Vinje* [2001a]. Interestingly, the three outlying melt duration years (1996, 2000, 2001 in Figures 12a–12b) were critical to statistical fit of the ice flux regression (Figure 12d). Apparently, disposition of the previous winter AO (through its putative effect on melt duration in FY ice) was generally inadequate for predicting January MY ice area following years when strong SLP gradients across the Fram Strait caused anomalously high ice export.

[51] When January MY ice area was regressed with both atmospheric parameters (previous winter AO and previous year Fram Strait SLP gradient), both contributed significantly to the model, which explained 75% of the interannual variation in MY ice area (Table 4). Although simplistic in construct, the model indicates that atmospheric conditions are closely tied to fluctuations in MY ice area through integrated linkages with both melt duration and export. Nevertheless, the model's statistical fit was fortuitously accentuated by highly variable atmospheric conditions during 1988–2001 [*Ostermeier and Wallace*, 2002], which contributed determinant extremities to the range of regressed observations.

[52] Accelerated losses in ice cover since 1989 [*Johannessen et al.*, 1995] have been attributed to a distinct regime shift in the Arctic's atmospheric circulation patterns. The 1989 shift marked transition into a sustained decade of anomalously positive wintertime Arctic Oscillation (AO) conditions [*Thompson and Wallace*, 1998]. The shift established lower atmospheric pressure over the Arctic, and was accompanied by warmer surface air temperatures [*Rigor et al.*, 2000; *Comiso*, 2002a] and numerous resultant changes in the sea ice environment [*Maslanik et al.*, 1996; *Deser et al.*, 2000; *Rigor et al.*, 2002; *Comiso et*

Table 4. January 1988–2001 Multiyear Ice Area (MY_a) Regressed on the Previous Winter's (JFM) Arctic Oscillation Index (AO) and the Previous Year's Average Sea Level Pressure Gradient (ΔSLP) Across the Fram Strait[a]

Parameter	Estimate	SE	S
AO (α)	−0.110	0.049	0.96
ΔSLP (β)	−0.177	0.034	>0.99
Intercept (χ)	4.235	0.166	>0.99

[a]For model $MY_a = \alpha(AO) + \beta(\Delta SLP) + \chi$, with R^2 = 0.75 and S > 0.99.

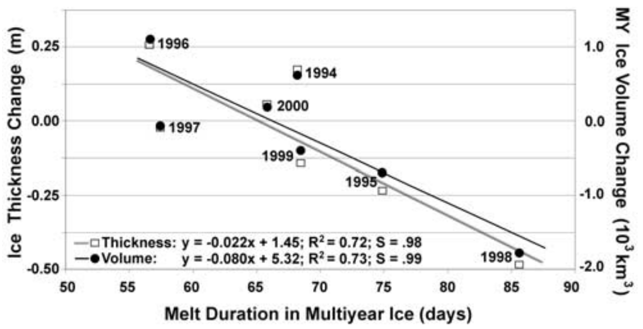

Figure 13. Consecutive winter mean ice thickness changes (adapted from *Laxon et al.* [2003, Figure 3b]) and consecutive January MY ice volume changes regressed on duration of the summer melt season in MY ice (1994–2001). Year labels denote the summer melt period.

al., 2003; *Belchansky et al.*, 2004]. Notably, the decade was punctuated in 1996 by a strong short-term phase reversal in the North Atlantic Oscillation [*Dickson et al.*, 2000] that apparently favored conditions for a large autumn recruitment of MY ice (Figure 8).

3.6. Thickness Changes

[53] Ice thickness is a difficult parameter to accurately monitor, yet is a sensitive factor in predictions of amplified Arctic warming [*Rind et al.*, 1995; *Holland and Bitz*, 2003]. Multiyear ice has been diminishing from the Arctic at rates 2–3 times greater than the annual average losses in total ice extent or area [*Johannessen et al.*, 1999; *Deser et al.*, 2000; *Parkinson and Cavalieri*, 2002; *Comiso*, 2002a, 2002b; *Vinnikov et al.*, 2002]. Disproportionate loss of MY ice infers net thinning and reduced volume of the ice pack, especially during periods with large interannual fluctuations in MY ice cover that would tend to increase the fraction of thinner second-year ice [*Comiso*, 2002b].

[54] Studies of submarine sea ice draft data have reported that accelerated thinning commenced in the late 1980s, concurrent with the AO regime shift [*Tucker et al.*, 2001; *Rothrock et al.*, 2003]. *Johannessen et al.* [1999] detected the same accelerated thinning using surface elastic-gravity wave measurements, and they also reported a strong annual correspondence between total MY ice area and thickness of the ice pack ($r \sim 0.82$, 1979–1991).

[55] Recent satellite altimeter measurements of Arctic sea ice freeboard have documented large interannual changes in mean ice thickness [*Laxon et al.*, 2003]. *Laxon et al.* [2003] analyzed altimetry data for areas with >1 m of estimated ice thickness within 65.0°N–81.5°N during eight winters (1993–2001), and reported a very high correlation (R^2 = 0.92) between the change in consecutive winter mean ice thickness and duration of the intervening melt season. Similarly, we correlated *Laxon et al.*'s [2003, Figure 3b] winter ice thickness changes with melt duration, but we used melt duration estimates derived with a different passive microwave algorithm [*Belchansky et al.*, 2004]. We also extended the analysis northward to 87.6°N, but restricted it to areas of predominantly multiyear ice [*Belchansky et al.*, 2004] because the method *Laxon et al.* [2003] used to estimate melt duration was only reliable in perennial ice [*Smith*, 1998]. Likewise, we found a significant (S = 0.98) but more modest correlation (R^2 = 0.72) between ice thickness change and melt duration. Our regression implied a 2.2-cm decrease in ice thickness for each day the melt season lengthened (Figure 13), compared to the 4.9 cm d^{-1} decrease reported by *Laxon et al.* [2003].

[56] We estimated annual change in MY ice volume by multiplying *Laxon et al.*'s [2003] consecutive winter ice thickness change with our neural network estimate of January MY ice area for the latter winter. When regressed on melt duration, an estimated 80 km^3 of MY ice diminished with each increasing day of summer melt (Figure 13). The large annual variations in volume thinning of MY ice attributed to summer melt are noteworthy because they're comparable in magnitude to annual variations in total volume export through the Fram Strait [*Vinje et al.*, 1998; *Kwok and Rothrock*, 1999], and higher than annual variations in total freshwater input from terrestrial rivers [*Shiklomanov et al.*, 2000; *Peterson et al.*, 2002]. Such pronounced short-term changes in MY ice volume caused by anomalous melt durations could disturb the freshwater balance and haline convection of the Arctic Ocean's upper layer [*Aagaard and Woodgate*, 2001; *Alekseev et al.*, 2003].

[57] *Laxon et al.*'s [2003] relatively short study period included two of the most extreme and thermodynamically opposed melt seasons (1996 and 1998) in a 23-year record (1979–2001) of observations [*Belchansky et al.*, 2004]. The second longest melt season in MY ice occurred in 1998, and was determinant to statistical significance of our correlations with thickness and volume changes (excluding 1998, R^2 = 0.41 and S = 0.87). The pronounced 1998 decrease in mean ice thickness (Figure 13) was not accompanied by a large decrease in MY ice area (Figure 8), substantiating a thermodynamic loss of ice volume. In contrast, 1996 had the shortest observed melt season in FY ice, and it preceded the largest annual increase in MY ice cover (Figure 8) and the largest consecutive year increase in *Laxon et al.*'s [2003] mean ice thickness fields (Figure 13). The extensive survival of FY ice during the short 1996 melt season caused a large recruitment of second-year ice that was likely responsible (at least in part) for *Laxon et al.*'s [2003] observed increase in mean ice thickness.

[58] Concurrent with the 1989 positive AO phase shift, interannual variability in melt duration shifted from relatively constant to highly fluctuating [*Belchansky et al.*, 2004]. The most anomalous melt seasons of the 1990s had significant impact on MY ice volume; reiterating the importance of thermodynamic processes to high-frequency changes in the Arctic's mass sea ice balance [*Laxon et al.*, 2003]. However, the importance of dynamic forces should not be overlooked, since they play a fundamental role in shaping the thermal regimes of the sea ice environment. During high-index AO winters, cyclonic wind and sea ice motion anomalies promote formation of thin ice and open leads [*Zhang et al.*, 2000; *Rigor et al.*, 2002] that enhance the heat flux from water, decrease the surface albedo, and amplify the summer melt through positive feedbacks [*Curry et al.*, 1995; *Rigor et al.*, 2000]. Hence, dynamic processes associated with winter AO conditions can imprint signatures that persist later into the year through their influences on spring melt and summer feedbacks [*Rigor et al.*, 2002].

During periods with stable melt duration, such as the low-index AO phase of the1980s [*Belchansky et al.*, 2004], thermodynamic forces are probably more constant and dynamic forces [*Arfeuille et al.*, 2000] probably dominate less variable changes in MY ice volume. Clearly, more research is necessary to decompose and better understand the complex interactions between dynamic and thermodynamic processes that control melt, recruitment, and transport of multiyear sea ice under different atmospheric circulation regimes and trends.

4. Conclusions

[59] Neural network algorithms were developed to estimate multiyear sea ice concentrations from SSM/I passive microwave brightness temperature data (19V, 19H, and 37V) during January 1988–2001. Neural networks are able to approximate a wide class of functions, without a priori assumptions about their distribution laws, and build decision surfaces of any configuration using a learning process. Here the neural networks accommodated important nonlinear relationships between the three-channel SSM/I emissivity signatures of multiyear ice and its surface area. Learning data for the neural networks utilized ice maps derived from Okean and ERS imagery in order to indirectly exploit the stability of multiyear ice signatures from active radar instruments [*Kwok et al.*, 1996]. After assessment of several topologies and learning algorithms, we concluded that networks learned with error back propagation and simulated annealing, under a 3-20-1 topology, produced the most consistent and physically plausible estimates of multiyear ice concentration.

[60] Interannual distributions of January multiyear ice were highly variable among the 14-year time series. While dense concentrations of multiyear ice were persistent in the western central Arctic, peripheral regions exhibited pronounced interannual fluctuations. Total area estimates of multiyear ice by the neural network method were intermediate to those of other passive microwave methods (which varied >40%), but the annual fluctuations and long-term trends were similar among all methods. Average January (1997–1999) multiyear ice concentration estimates by the neural network method were only slightly less (0.9–2.5%) than corresponding estimates derived from Radarsat data in the Beaufort-Chukchi Seas, indicating that the network's use of Okean and ERS learning data afforded good continuity between multiyear ice retrievals from passive microwave and those from active radar instruments.

[61] During 1988–2001, total January multiyear ice area in the Arctic declined at a significant linear rate of -54.3×10^3 km^2 yr^{-1} (-1.4% yr^{-1}). Peripheral regions exhibited variable rates of decline with pronounced interannual fluctuations. Associations with atmospheric circulation patterns were evident. The most extensive and persistent decline in January multiyear ice occurred in the southern Beaufort and Chukchi Seas, where average concentrations dropped 3.3% yr^{-1} in probable response to cyclonic atmospheric circulation anomalies that have weakened the Beaufort Gyre during the past decade [*Drobot and Maslanik*, 2003]. In 1996, a short-term phase reversal in atmospheric circulation patterns [*Dickson et al.*, 2000] coincided with a very large recruitment (>10^6 km^2) that replenished most of the multiyear ice in the Arctic Basin, but accelerated declines during 1997–2001 offset the 1996 recruitment.

[62] Spatial and temporal variations of the Arctic's multiyear ice cover manifest complex integrations of seasonal ice recruitment, melt, and transport. Atmospheric circulation patterns appeared to have controlling influences on both the dynamic and thermodynamic processes affecting changes in the perennial ice pack [*Zhang et al.*, 2000; *Dumas et al.*, 2003]. The Arctic Oscillation index and the sea level pressure gradient across the Fram Strait accounted for 75% of the 1988–2001 variability in multiyear ice area fluctuations through their putative associations with duration of the summer melt season and ice export, respectively. Melt duration also had significant influence on volume changes in multiyear ice, corroborating the importance of thermodynamic processes to short-term changes in the Arctic's mass sea ice balance [*Laxon et al.*, 2003], although the importance of dynamic processes in preconditioning the thermal environment [*Rigor et al.*, 2002] should not be overlooked.

[63] Our 14-year analysis of multiyear ice dynamics is insufficient to project long-term trends. Whether recent declines in multiyear ice area and thickness are indicators of anthropogenic exacerbations to positive feedbacks that will lead the Arctic to an unprecedented future of reduced ice cover [*Vinnikov et al.*, 1999; *Comiso*, 2002b; *Johannessen et al.*, 2004], or whether they are simply ephemeral expressions of natural low frequency oscillations [*Vinje*, 2001b; *Polyakov et al.*, 2002, 2003] bears significant ramifications to Arctic ecology and global climate that clearly warrants continued scientific investment.

[64] **Acknowledgments.** This work was carried out with the support of the International Arctic Research Center and Cooperative Institute for Arctic Research, University of Alaska Fairbanks, and the NATO Scientific Affairs Division (Collaborative Linkage grant EST.CLG.978230). We would like to acknowledge the Alaska SAR Facility (Fairbanks) for providing ERS-1 sea-ice concentrations, the National Snow and Ice Data Center (University of Colorado) for providing the SSM/I Daily Polar Gridded Tb and Sea Ice Concentrations, and the NASA Jet Propulsion Laboratory for supplying the RGPS products. The authors also thank I. Mordvintsev (Institute of Ecology and Evolution, RAS) for his dedicated contributions to this work.

References

Aagaard, K., and R. A. Woodgate (2001), Some thoughts on the freezing and melting of sea ice and their effects on the ocean, *Ocean Modell.*, *3*, 127–135.
Abdalati, W., K. Steffen, C. Otto, and K. Jezek (1995), Comparison of brightness temperatures from SSM/I instruments on the DMSP F8 and F11 satellites for Antarctica and the Greenland ice sheet, *Int. J. Remote Sens.*, *16*, 1223–1229.
Agnew, I. (1993), Simultaneous winter sea-ice and atmospheric circulation anomaly patterns, *Atmos. Ocean*, *31*, 259–280.
Alekseev, G. V., O. M. Johannessen, A. A. Korablev, and A. Proshutinsky (2003), Arctic Ocean and sea ice, in *Arctic Environment Variability in the Context of Global Change*, edited by L. P. Bobylev, K. Y. Kondratyev, and O. M. Johannessen, pp. 107–202, Praxis, Chichester, UK.
Arfeuille, G. L., A. Mysak, and L. B. Tremblay (2000), Simulation of the interannual variability of the wind-driven Arctic sea-ice cover during 1958–1998, *Clim. Dyn.*, *16*, 107–121.
Ball, G. H., and D. J. Hall (1967), A clustering technique for summarizing multivariate data, *Behavioral Sci.*, *12*, 153–155.
Barry, R. G. (1990), Observational evidence of changes in global snow and ice cover, in *Observed Climate Variations and Change: Contribution in Support of Section 7 of the 1990 IPCC Scientific Assessment*, edited by D. E. Parker, pp. 1.1–1.20, Cambridge Univ. Press, New York.
Barry, R. G., M. C. Serreze, J. A. Maslanik, and R. H. Preller (1993), The Arctic sea ice-climate system: Observations and modeling, *Rev. Geophys.*, *31*, 397–422.

Barton, S. A. (1991), A matrix method for optimizing a neural network, *Neural Comput.*, *3*, 450–459.
Belchansky, G. I., and D. C. Douglas (2000), Classification methods for monitoring Arctic sea-ice using Okean passive/active two-channel microwave data, *Remote Sens. Environ.*, *73*, 307–322.
Belchansky, G. I., and D. C. Douglas (2002), Seasonal comparisons of sea ice concentration estimates derived from SSM/I, Okean, and Radarsat data, *Remote Sens. Environ.*, *81*, 67–81.
Belchansky, G. I., D. C. Douglas, and N. G. Platonov (2004), Duration of the Arctic sea ice melt season: Regional and interannual variability, 1979–2001, *J. Clim.*, *17*, 67–80.
Boyd, T. J., M. Steele, R. D. Muench, and J. T. Gunn (2002), Partial recovery of the Arctic Ocean halocline, *Geophys. Res. Lett.*, *29*(14), 1657, doi:10.1029/2001GL014047.
Cavalieri, D. J., B. A. Burns, and R. G. Onstott (1990a), Investigation of the effects of summer melt on the calculation of sea ice concentration using active and passive microwave data, *J. Geophys. Res.*, *95*, 5339–5369.
Cavalieri, D., P. Gloerson, and J. Zwally (1990b), DMSP SSM/I daily polar gridded sea ice concentrations, edited by J. Maslanik and J. Stroeve, report, Natl. Snow and Ice Data Cent., Boulder, Colo. (Update 2003 available at nsidc.org/data/nsidc-0002.html)
Cavalieri, D., J. Crawford, M. R. Drinkwater, D. T. Eppler, L. D. Farmer, R. R. Jentz, and C. C. Wackerman (1991), Aircraft active and passive microwave validation of sea ice concentration from the Defense Meteorological Satellite Program special sensor microwave imager, *J. Geophys. Res.*, *96*, 21,989–22,008.
Cavalieri, D. J., C. L. Parkinson, P. Gloersen, J. C. Comiso, and H. J. Zwally (1999), Deriving long-term time series of sea ice cover from satellite passive-microwave multisensor data sets, *J. Geophys. Res.*, *104*, 15,803–15,814.
Chapman, W. L., and J. E. Walsh (1993), Recent variations of sea ice and air temperature in high latitudes, *Bull. Am. Meteorol. Soc.*, *74*, 33–47.
Comiso, J. (1990a), DMSP SSM/I daily polar gridded sea ice concentrations, edited by J. Maslanik and J. Stroeve, report, Natl. Snow and Ice Data Cent., Boulder, Colo. (Update 2003 available at nsidc.org/data/nsidc-0002.html)
Comiso, J. C. (1990b), Arctic multiyear ice classification and summer ice cover using passive microwave satellite data, *J. Geophys. Res.*, *95*, 13,411–13,422.
Comiso, J. C. (2001), Satellite-observed variability and trend in sea-ice extent, surface temperature, albedo and clouds in the Arctic, *Ann. Glaciol.*, *33*, 457–473.
Comiso, J. C. (2002a), Correlation and trend studies of the sea-ice cover and surface temperatures in the Arctic, *Ann. Glaciol.*, *34*, 420–428.
Comiso, J. C. (2002b), A rapidly declining perennial sea ice cover in the Arctic, *Geophys. Res. Lett.*, *29*(20), 1956, doi:10.1029/2002GL015650.
Comiso, J. C., and R. Kwok (1996), Surface and radiative characteristics of the summer Arctic sea ice cover from multisensor satellite observations, *J. Geophys. Res.*, *101*, 28,397–28,416.
Comiso, J. C., D. J. Cavalieri, C. L. Parkinson, and P. Gloersen (1997), Passive microwave algorithms for sea ice concentration: Comparison of two techniques, *Remote Sens. Environ.*, *60*, 357–384.
Comiso, J. C., J. Yang, S. Honjo, and R. A. Krishfield (2003), Detection of change in the Arctic using satellite and in situ data, *J. Geophys. Res.*, *108*(C12), 3384, doi:10.1029/2002JC001347.
Curry, A. J., J. L. Schramn, and E. E. Ebert (1995), On the ice albedo climate feedback mechanism, *J. Clim.*, *8*, 240–247.
Deser, C., and M. L. Blackmon (1993), Surface climate variation over the North Atlantic Ocean during winter: 1900–1989, *J. Clim.*, *6*, 1743–1753.
Deser, C., J. E. Walsh, and M. S. Timlin (2000), Arctic sea ice variability in the context of recent atmospheric circulation trends, *J. Clim.*, *13*, 617–633.
Deser, C., M. Holland, G. Reverdin, and M. Timlin (2002), Decadal variations in Labrador Sea ice cover and North Atlantic sea surface temperatures, *J. Geophys. Res.*, *107*(C5), 3035, doi:10.1029/2000JC000683.
Dickson, R. R., T. J. Osborn, J. W. Hurrell, J. Meincke, J. Blindheim, B. Adlandsvik, T. Vinje, G. Alekseev, and W. Maslowski (2000), The Arctic Ocean response to the North Atlantic oscillation, *J. Clim.*, *13*, 2671–2696.
Drobot, S. D., and J. A. Maslanik (2003), Interannual variability in summer Beaufort Sea ice conditions: Relationship to winter and summer surface and atmospheric variability, *J. Geophys. Res.*, *108*(C7), 3233, doi:10.1029/2002JC001537.
Dumas, J. A., G. M. Flato, and A. J. Weaver (2003), The impact of varying atmospheric forcing on the thickness of arctic multi-year sea ice, *Geophys. Res. Lett.*, *30*(18), 1918, doi:10.1029/2003GL017433.
Emery, W. J., C. Fowler, and J. A. Maslanik (1994), Arctic sea ice concentrations from special sensor microwave imager and advanced very high resolution radiometer satellite data, *J. Geophys. Res.*, *99*, 18,329–18,342.
Erlingsson, B. (1988), Two-dimensional deformation patterns in sea ice, *J. Glaciol.*, *34*, 301–308.
Ezraty, R., and A. Cavanié (1999), Intercomparison of backscatter maps over Arctic sea ice from NSCAT and the ERS scatterometer, *J. Geophys. Res.*, *104*, 11,471–11,483.
Fang, Z., and J. M. Wallace (1994), Arctic sea ice variability on a timescale of weeks: Its relation to atmospheric forcing, *J. Clim.*, *7*, 1897–1913.
Fetterer, F., D. Gineris, and R. Kwok (1994), Sea-ice type maps from Alaska Synthetic Aperture Radar Facility imagery: An assessment of Arctic multiyear ice coverage estimated through Alaska SAR Facility data analysis, *J. Geophys. Res.*, *99*, 22,443–22,458.
Fung, A. K. (1994), *Microwave Scattering and Emission Models and Their Applications*, 573 pp., Artech House, Norwood, Mass.
Gloersen, P., and D. J. Cavalieri (1986), Reduction of weather effects in the calculation of sea ice concentration from microwave radiances, *J. Geophys. Res.*, *91*, 3913–3919.
Gloersen, P., C. L. Parkinson, D. J. Cavalieri, J. C. Comiso, and H. J. Zwally (1999), Spatial distribution of trends and seasonality in the hemispheric sea ice covers: 1978–1996, *J. Geophys. Res.*, *104*, 20,827–20,835.
Grenfell, T. C. (1992), Surface-based passive microwave studies of multiyear sea ice, *J. Geophys. Res.*, *97*, 3485–3501.
Grody, N. C. (1988), Surface identification using satellite microwave radiometers, *IEEE Trans. Geosci. Remote Sens.*, *26*, 850–859.
Grotefendt, K., K. Logemann, D. Quadfasel, and S. Ronski (1998), Is the Arctic Ocean warming?, *J. Geophys. Res.*, *103*, 27,679–27,687.
Gunn, J. T., and R. D. Muench (2001), Observed changes in Arctic Ocean temperature structure over the past half decade, *Geophys. Res. Lett.*, *28*, 1035–1038.
Hecht-Nielsen, R. (1987), Kolmogorov's mapping neural network existence theorem, *Proc. IEEE Intern. Conf. on Neural Networks*, *3*, 11–14.
Hewitt, C. D., C. A. Senior, and J. F. Mitchell (2001), The impact of dynamic sea-ice on the climatology and climate sensitivity of GCM, a study of past, present, and future climates, *Clim. Dyn.*, *17*, 655–668.
Hibler, W. D., and R. Becky (1985), Numerical simulation of Northern Hemisphere sea ice variability, 1951–1980, *J. Geophys. Res.*, *90*, 4847–4865.
Holland, D. M. (2001), An impact of subgrid-scale ice-ocean dynamics on sea-ice cover, *J. Clim.*, *14*, 1585–1601.
Holland, M. M., and C. M. Bitz (2003), Polar amplification of climate change in coupled models, *Clim. Dyn.*, *21*, 221–232.
Holland, M. M., and J. A. Curry (1999), The role of physical processes in determining the interdecadal variability of central Arctic sea ice, *J. Clim.*, *12*, 3319–3330.
Holland, M. M., J. A. Curry, and J. L. Schramm (1997), Modeling the thermodynamics of a sea ice thickness distribution: 2. Sea ice/ocean interactions, *J. Geophys. Res.*, *102*, 23,093–23,107.
Holloway, G., and T. Sou (2002), Has Arctic sea ice rapidly thinned?, *J. Clim.*, *15*, 1691–1701.
Johannessen, O. M., M. Miles, and E. Bjorgo (1995), The Arctic's shrinking sea ice, *Nature*, *376*, 126–127.
Johannessen, O. M., E. S. Shalina, and M. W. Miles (1999), Satellite evidence for an Arctic sea ice cover in transformation, *Science*, *286*, 1937–1939.
Johannessen, O. M., et al. (2004), Arctic Climate change: Observed and modelled temperature and sea ice variability, *Tellus, Ser. A*, *56*, 1–18.
Kalman, R. E., and R. S. Bucy (1961), New results in linear filtering and prediction theory, *J. Basic Eng.*, *83*, 95–108.
Kirkpatrick, S. (1983), Optimization by simulated annealing, *Science*, *220*, 671–680.
Kukla, G. (2004), Central Arctic: Battleground of natural and man-made climate forcing, *Eos Trans. AGU*, *85*(20), 200–202.
Kwok, R., and G. F. Cunningham (1993), Alaska SAR Facility Geophysical Processor System data user's handbook, version 2, *JPL D-9526*, Natl. Aeronaut. and Space Admin., Jet Propul. Lab., Pasadena, Calif.
Kwok, R., and G. F. Cunningham (2002), Seasonal ice area and volume production of the Arctic Ocean: November 1996 through April 1997, *J. Geophys. Res.*, *107*(C10), 8038, doi:10.1029/2000JC000469.
Kwok, R., and D. A. Rothrock (1999), Variability of Fram Strait ice flux and North Atlantic Oscillation, *J. Geophys. Res.*, *104*, 5177–5189.
Kwok, R., E. Rignot, B. Holt, and R. G. Onstott (1992), Identification of sea ice type in spaceborne SAR data, *J. Geophys. Res.*, *97*, 2391–2402.
Kwok, R., J. C. Comiso, and G. F. Cunningham (1996), Seasonal characteristics of the perennial ice cover of the Beaufort Sea, *J. Geophys. Res.*, *101*, 28,417–28,439.
Laxon, S., N. Peacock, and D. Smith (2003), High interannual variability of sea ice thickness in the Arctic region, *Nature*, *425*, 947–950.
Lindsay, R. W. (1998), Temporal variability in the energy balance of thick Arctic pack ice, *J. Clim.*, *11*, 313–331.

Manabe, S., M. J. Spelman, and R. J. Stouffer (1992), Transient responses of a coupled ocean atmosphere model to gradual changes in atmospheric CO_2, *J. Clim.*, *5*, 105–126.
Martinson, D. G., and M. Steele (2001), Future of the Arctic sea ice cover: Implications of an Antarctic analog, *Geophys. Res. Lett.*, *28*, 307–310.
Maslanik, J. A. (1992), Effects of weather on the retrieval of sea ice concentration and ice type from passive microwave data, *Int. J. Remote Sens.*, *13*, 37–54.
Maslanik, J. A., and M. C. Serreze (1999), On the record reduction in 1998 western Arctic sea-ice cover, *Geophys. Res. Lett.*, *26*, 1905–1908.
Maslanik, J., and J. Stroeve (1992), DMSP SSM/I Daily Polar Gridded Brightness Temperatures [CD-ROM], Natl. Snow and Ice Data Cent., Boulder, Colo.
Maslanik, J. A., M. C. Serreze, and R. G. Barry (1996), Recent decreases in Arctic summer ice cover and linkages to atmospheric circulation anomalies, *Geophys. Res. Lett.*, *23*, 1677–1680.
Mysak, L. A., R. G. Ingram, J. Wang, and A. Van Der Baaren (1996), The anomalous sea-ice extent in Hudson Bay, Baffin Bay and the Labrador Sea during three simultaneous ENSO and NAO episodes, *Atmos. Ocean*, *34*, 313–343.
Ostermeier, G. M., and J. M. Wallace (2002), Trends in the North Atlantic oscillation-Northern Hemisphere annular mode during the twentieth century, *J. Clim.*, *16*, 336–341.
Parkinson, C. L., and D. J. Cavalieri (2002), A 21 year record of Arctic sea-ice extents and their regional, seasonal and monthly variability and trends, *Ann. Glaciol.*, *34*, 441–446.
Parkinson, C. L., D. J. Cavalieri, P. Gloersen, H. J. Zwally, and J. C. Comiso (1999), Arctic sea ice extents, areas, and trends, 1978–1996, *J. Geophys. Res.*, *104*, 20,837–20,856.
Parkinson, C. L., D. Rind, G. J. Healy, and D. G. Martinson (2001), The impact of sea ice concentration accuracies on climate model simulations with the GISS GCM, *J. Clim.*, *14*, 2606–2623.
Perovich, D. K., T. C. Grenfell, J. A. Richter-Menge, B. Light, W. B. Tucker III, and H. Eicken (2003), Thin and thinner: Sea ice mass balance measurements at SHEBA, *J. Geophys. Res.*, *108*(C3), 8050, doi:10.1029/2001JC001079.
Peterson, B. J., R. M. Holmes, J. W. McClelland, C. J. Vörösmarty, R. B. Lammers, A. I. Shiklomanov, I. A. Shiklomanov, and S. Rahmstorf (2002), Increasing river discharge to the Arctic Ocean, *Science*, *298*, 2171–2173.
Polyakov, I. V., M. A. Johnson, R. L. Colony, U. Bhatt, and G. V. Alekseev (2002), Observationally based assessment of polar amplification of global warming, *Geophys. Res. Lett.*, *29*(18), 1878, doi:10.1029/2001GL011111.
Polyakov, I. V., G. V. Alekseev, R. V. Bekryaev, U. S. Bhatt, R. Colony, M. A. Johnson, V. P. Karklin, D. Walsh, and A. V. Yulin (2003), Long-term ice variability in Arctic marginal seas, *J. Clim.*, *16*, 2078–2085.
Rigor, I. G., R. L. Colony, and S. Martin (2000), Variations in surface air temperature observations in the Arctic, 1979–97, *J. Clim.*, *13*, 896–914.
Rigor, I. G., J. M. Wallace, and R. L. Colony (2002), Response of sea ice to the Arctic Oscillation, *J. Clim.*, *15*, 2648–2663.
Rind, D., R. Healy, C. Parkinson, and D. Martinson (1995), The role of sea ice in $2 \times CO_2$ climate model sensitivity: 1. The total influence of sea ice thickness and extent, *J. Clim.*, *8*, 449–463.
Rind, D., R. Healy, C. Parkinson, and D. Martinson (1997), The role of sea ice in $2 \times CO_2$ climate model sensitivity: 2. Hemispheric dependencies, *Geophys. Res. Lett.*, *24*, 1491–1494.
Rothrock, D. A., J. Zhang, and Y. Yu (2003), The Arctic ice thickness anomaly of the 1990s: A consistent view from observations and models, *J. Geophys. Res.*, *108*(C3), 3083, doi:10.1029/2001JC001208.
Serreze, M. C., et al. (2003), A record minimum arctic sea ice extent and area in 2002, *Geophys. Res. Lett.*, *30*(3), 1110, doi:10.1029/2002GL016406.
Shiklomanov, I. A., A. I. Shiklomanov, R. B. Lammers, B. J. Peterson, and C. J. Vörösmarty (2000), The dynamics of river water inflow to the Arctic Ocean, in *The Freshwater Budget of the Arctic Ocean*, edited by E. L. Lewis, pp. 281–296, Kluwer Acad., Norwell, Mass.
Smith, D. M. (1998), Observation of perennial Arctic sea ice melt and freeze-up using passive microwave data, *J. Geophys. Res.*, *103*, 27,753–27,769.
Steele, M., and T. Boyd (1998), Retreat of the cold halocline layer in the Arctic Ocean, *J. Geophys. Res.*, *103*, 10,419–10,435.
Steele, M., et al. (2001), Adrift in the Beaufort Gyre: A model intercomparison, *Geophys. Res. Lett.*, *28*, 2935–2938.
Stroeve, J., J. Maslanik, and L. Xiaoming (1998), An intercomparison of DMSP F11- and F13- derived sea ice products, *Remote Sens. Environ.*, *64*, 132–152.
Svendsen, E., K. Kloster, B. Farrelly, O. M. Johannessen, J. A. Johannessen, W. J. Campbell, P. Gloersen, D. Cavalieri, and C. Mätzler (1983), Norwegian remote sensing experiment: Evaluation of the Nimbus 7 scanning multichannel microwave radiometer for sea ice research, *J. Geophys. Res.*, *88*, 2781–2991.
Thomas, D. N., and G. S. Dieckmann (Eds.) (2003), *Sea ice—An Introduction to its Physics, Chemistry, Biology and Geology*, 402 pp., Iowa State Univ. Press, Ames.
Thompson, D. W. J., and J. W. Wallace (1998), The Arctic Oscillation signature in the wintertime geopotential height and temperature fields, *Geophys. Res. Lett.*, *25*, 1297–1300.
Tooma, S. G., R. A. Mennella, J. P. Hollinger, and R. D. Ketchum (1975), Comparison of sea-ice identification between airborne dual-frequency passive microwave radiometry and standard laser/infrared techniques, *J. Glaciol.*, *15*, 225–239.
Tucker, W. B., III, D. K. Perovich, A. J. Gow, W. F. Weeks, and M. R. Drinkwater (1992), Physical properties of sea ice relevant to remote sensing, in *Microwave Remote Sensing of Sea Ice*, *Geophys. Monogr. Ser.*, vol. 68, edited by F. D. Carsey, pp. 9–28, AGU, Washington, D. C.
Tucker, W. B., III, J. W. Weatherly, D. T. Eppler, D. Farmer, and D. L. Bentley (2001), Evidence for rapid thinning of sea ice in the western Arctic Ocean at the end of the 1980s, *Geophys. Res. Lett.*, *28*, 2851–2854.
Tzeng, Y. C., K. S. Chen, W. L. Kao, and A. K. Fung (1994), A dynamic learning neural network for remote sensing application, *IEEE Trans. Geosci. Remote Sens.*, *32*, 1096–1102.
Vinje, T. (2001a), Fram Strait ice fluxes and atmospheric circulation: 1950–2000, *J. Clim.*, *14*, 3508–3517.
Vinje, T. (2001b), Anomalies and trends of sea-ice extent and atmospheric circulation in the Nordic Seas during the period 1864–1998, *J. Clim.*, *14*, 255–267.
Vinje, T., N. Nordlund, and A. Kvambekk (1998), Monitoring ice thickness in Fram Strait, *J. Geophys. Res.*, *103*, 10,437–10,449.
Vinnikov, K. Y., A. Robock, R. J. Stouffer, J. E. Walsh, C. L. Parkinson, D. J. Cavalieri, J. F. B. Mitchell, D. Garrett, and V. F. Zakharov (1999), Global warming and Northern Hemisphere sea ice extent, *Science*, *286*, 1934–1937.
Vinnikov, K. Y., A. Robock, D. J. Cavalieri, and C. L. Parkinson (2002), Analysis of seasonal cycles in climatic trends with application to satellite observations of sea ice extent, *Geophys. Res. Lett.*, *29*(9), 1310, doi:10.1029/2001GL014481.
Walsh, J. E., and C. M. Johnson (1979), An analysis of arctic sea ice fluctuations, 1953–1977, *J. Phys. Oceanogr.*, *9*, 580–591.
Winsor, P. (2001), Arctic sea ice thickness remained constant during the 1990s, *Geophys. Res. Lett.*, *28*, 1039–1041.
Zhang, J., D. A. Rothrock, and M. Steele (1998), Warming of the Arctic Ocean by a strengthened Atlantic inflow: Model results, *J. Geophys. Res.*, *25*, 1745–1748.
Zhang, J., D. A. Rothrock, and M. Steele (2000), Recent changes in the Arctic sea ice: The interplay between ice dynamics and thermodynamics, *J. Clim.*, *13*, 3099–3114.

I. V. Alpatsky, G. I. Belchansky, and N. G. Platonov, Space Monitoring and Ecoinformation Systems Sector, Institute of Ecology, Russian Academy of Sciences, Leninsky Prospect 33, Moscow, Russia 119071. (belchans@eimb.ru)

D. C. Douglas, USGS Alaska Science Center, Juneau Field Station, 3100 National Park Road, Juneau, AK 99801, USA. (david_douglas@usgs.gov)